ABSTRACT

Title of Thesis:	EVALUATION OF IMPACT OF NOVEL BARRIER COATINGS ON FLAMMABILITY OF A STRUCTURAL AEROSPACE COMPOSITE THROUGH EXPERIMENTS AND MODELING
	Lucas Summerfield Crofton, Masters of Science, 2021
Thesis Directed By:	Dr. Stanislav Stoliarov, Associate Professor, Department of Fire Protection Engineering

Composites have become a integral part of the structure of airplanes, and their use within aircraft continues to grow as composites continue to improve. While polymer composites are an improvement in many facets to traditional airspace materials, their flammability is something called into question. The work performed for this study was to create a pyrolysis model for a particular aerospace composite, IM7 graphite fiber with Cytec 5250-4 Bismaleimide matrix (BMI), and three innovative composite barrier coatings that could be applied to the BMI to potentially improve its performance in fire scenarios. The composites were all tested individually, in a series of milligram-scale tests, and the test results were inversely

analyzed to determine stoichiometry, chemical kinetics, and thermodynamics of their thermal decomposition and combustion. Gram-scale experiments using the Controlled Atmosphere Pyrolysis Apparatus II (CAPA II) were performed on the BMI by itself and then again with one of each of the composite barrier coatings applied in a defined thickness. This data were inversely analyzed to define the thermal conductivity of the sample and resolve it's emissivity. It was found after fully defining a pyrolysis model for each composite material that the composite barrier coatings did not provide any benefit to the base composite BMI, and only added more fuel load which in turn contributed to a increase in heat release rate when computational simulations were run to mimic a airplane fuel fire.

EVALUATION OF IMPACT OF NOVEL BARRIER COATINGS ON FLAMMABILITY OF A STRUCTURAL AEROSPACE COMPOSITE THROUGH EXPERIMENTS AND MODELING

by

Lucas Summerfield Crofton

Thesis submitted to the Faculty of the Graduate School of the
University of Maryland, College Park, in partial fulfillment
of the requirements for the degree of
Master of Science
2021

Advisory Committee:
Professor Stanislav Stoliarov, Ph.D., Chair
Professor Arnuad Trouvé
Mark McKinnon

Acknowledgements

I must first thank my advisor, Dr. Stanislav Stoliarov. The guidance and patience you had shown me throughout the process of my research was invaluable to say the least, especially in light of this tough past year. I feel more confidence now moving forward with my career thanks to the high standards and quality of work you have instilled in me.

I would like to acknowledge and thank Dr. Trouve and Mark McKinnon for serving as members on my thesis committee. I appreciate you both taking the time out of your busy schedules to review and provide comments on my work.

My research would not have been accomplished without the help and support that I received from my lab group. I have to thank Dushyant, Conor, Jacques, and Will for helping me throughout this process, whether it was explaining a concept to me, validating collected data and constructed plots, providing comments on my writing, or just shooting the breeze for a few minutes to take our minds off work. I greatly appreciated it all and am thankful to have worked with each of you so closely.

My family has always been a large part of my life and I owe a lot to them for helping shaping me into the person I am today. My Mom, Dad, my sister, Sydney, and my brother, Lane, have supported me tirelessly throughout my college career, and even more so as a graduate student. They have always been my number one supporters, whether it be listening to me venting when something wasn't working or listening to me explain a MatLab script I had written for the 100th time. I cannot thank you all enough, I look forward to celebrating this achievement with all of you.

I would be reminisced if I did not thank my grandparents, Nana and Pappy, for their unrelenting support. Your constant interest in my thesis and constant positive attitude no matter the circumstance was a constant source of warmth and encouragement for me. I cannot thank you both enough.

I would like to thank NAVAIR for funding my research through the award N00421-19-2-0001. I would also like to extend my thanks and gratitude to Dr. Ray Meilunas as my contact within my sponsor of NAVAIR. Your work and insight was appreciated, especially considering the tough circumstances of the past year.

There are many people that deserve my thanks for all of the help they have provided me during my time as a graduate student pursuing my Masters of Science. I extend my gratitude to those I may not have explicitly listed here, friends, family, coworkers, and many more. Thank you all for your support.

Table of Contents

List of Tables

List of Figures

Chapter 1: Introduction

1.1 Background and Motivation

Aircraft are a feat of engineering and are utilized in many different facets. Aircraft are used for civil and military purposes that include both foreign and domestic travel. As with any mode of transportation it is important to understand the structural components that make up the vehicle to understand its limitations. When the aircraft started becoming a viable manufactured vehicle, they were mainly constructed out of light weight wood and wire braced structures, this then was replaced with lightweight metal structures [1]. This advancement was achieved due to material science and aerospace engineering evolving over the past century [1]. The most recent achievement has been the transition from light weight metal materials to polymers [1-3]. The drive towards this transition has been fueled by the weight saving abilities of replacing metals used in planes with polymers, a plane could save between 25 – 45% of the weight from its metal predecessors [4]. With less weight involved on an aircraft it allows for better fuel economy.

Polymers can be found throughout an aircraft in its interior, frame and structural components such as the fuselage [3]. In terms of the structural components of an aircraft, some of the polymers utilized are shape-memory polymers, reinforced polymers, and composites [3, 5, 6]. Shape-memory polymers are commonly utilized as a flexible yet durable material to be implemented as the skin of the aircraft that can shift and morph in shape [6, 7]. Reinforced polymers are used for their mechanical properties especially when utilized within electrically driven aircraft [8]. Polymers

have found widespread use due to their strength to weight ratio, chemical resistance, and electrical insulating properties, among others [9, 10]. Composites made with polymers look to capitalize on these beneficial mechanical and chemical properties [11]. With these properties used to make up composite materials it becomes evident why these materials have been replacing light weight metals like titanium and aluminum in aircraft at rapid rates [4, 12]. The focus of this work will be on composites, more specifically polymer matrix composites used within aircraft.

A composite material is defined as a multi-component and multi-phase system that is made up of two or more materials in a non-homogenous manner with favorable synergism [13]. A composite material is broken down into three separate phases, the matrix, reinforcement, and interface phase or interphase. The matrix phase is defined as the continuous portion of the composite. The reinforcement phase is that which surrounds the matrix and scattered among the composite. The final phase, the interphase, is the interface between the matrix and reinforcement phases. Composites are commonly classified by the matrix material which is where the term polymer matrix composite (PMC) comes from [13]. Composites, in this case, are chosen because as stated before they provide the characteristics of both their matrix and reinforcement phases while providing improvement to some characteristics when comparing to the separate phases individually. PMC's perform well in a number categories that promote their high stiffness, high strength, shear strength, and low density [12]. However, they tend to fall short when it comes to their flammability in comparison to their non-flammable counterparts of aluminum and titanium used in aircraft. This holds true for both the matrix and the reinforcement phase. When

combined as they are in a composite, their flammability characteristics tend to compound just as their beneficial mechanical properties do. This synergism becomes important to consider when dealing with aircrafts and the extreme exposure conditions of these materials. The thermal degradation of these materials or the exposure of these materials to fire may compromise that aircraft. It is therefore important to understand the flammability of these materials. A fully developed pyrolysis model will provide this understanding by providing a defined insight in the chemical and physical phenomena taking place while the composite is exposed to heat flux.

A pyrolysis model is mathematical model that takes the physical aspects of a material and the chemical reactions taking place within the given material and relates them to the processes of heat transfer and subsequent mass loss of the given material. This enables a more accurate understanding of how that material may respond in multiple fire scenarios. Modeling tools have been developed include: Gypro [14], NIST Fire Dynamics Simulator [15], and ThermaKin [16,17,18]. All of these models require input from the user that defines the material properties for each material included within the model. These properties are then used to describe the chemical kinetics and thermodynamic behaviors of the material. These properties include the mass loss kinetics parameters, heat capacities, reaction order, stoichiometry, and conductivity to name but a few. It is very important that these properties are well understood and accurately quantified with a level of certainty such to ensure the predictive model is representative of what would occur if compared to a replicated test mimicking the environment defined by the model, for both a bench scale or full

scale test. These properties are quantified utilizing different laboratory-scale experiments.

The driving force for the development of a pyrolysis model for composite materials being used within airplanes is the large increase of their usage within aircraft since their introduction [1,19]. Since 1987 the usage of structural composites in aircraft has risen from 1-2% of the total mass of the structural components to just above 50% as of 2013 [19,20]. More recent data over the past decade has shown that the 50% value has held true as most recently reported by Boeing for their 787 airliners [21]. With this increase in composite material, there comes the benefits of a lighter aircraft allowing for better fuel efficiency [19, 20] but the fact that 50% of the structural components mass within the aircraft is now constructed of a flammable material needs to be taken into consideration. With such a large portion of aircrafts now being comprised of composites there has not been a well-developed database, making the development of a fully developed pyrolysis model even more important for each new composite introduced for aircraft.

1.2 Previous Works

When a new material is considered for use in a system, the material should undergo rigorous testing to accurately quantify the validity of the material for a predefined use. This holds true for any system or device, aircraft included. To address this issue and hazard, test methods have been developed and research has been conducted with the intention of better quantifying the flammability characteristics of PMC. The determination of these flammability characteristics has evolved over time, and this is discussed here.

The FAA released a compiled handbook on the multitude of material fire tests used within the industry to determine the viability of a material to be used within an aircraft based on how well it performed in a fire environment [22]. The tests described within the handbook are specified for certain components of the aircraft, one test may not be used for all components of an aircraft. These tests are taken directly from the Federal Aviation Regulation (FAR) 25 [23]. The focus of these tests ranges from the cabin and cargo compartment materials, the electrical wires, the slides, ramps, and rafts used on the aircraft [22].

There are two tests from the FAA handbook [22] that would be most commonly used for a PMC based on the components they test: The Vertical and Horizontal Bunsen Burner tests for cabin and cargo compartment materials, and the Heat Release Rate Test for Cabin Materials [22]. The Bunsen burner tests are conducted in different orientations to see how long a specimen will stay ignited when a specimen of at least 3 inches by 12 inches is exposed to a bunsen burner for 12 to 60 seconds [22]. The time the material stays aflame is recorded along with the number of pieces of the specimen that have fallen off the original prepared sample and how long they also stayed lit. The Heat Release Rate test [22] for cabin materials is a similar testing method to that of the cone calorimeter where the sample is placed within a chamber and subjected to a given heat flux, in this case 3.5 W cm^{-2} [22]. The gases are then burned using pilot flames above the sample and the temperature difference is used along with a calibration factor to determine the heat release rate (HRR) of the sample. Between these three test methods, there is an understanding of the HRR of a given sample, and its general ignition time and duration of flame for a

specified sample size. This data generated from all three tests does provide insight into the materials flammability, but part of that data is qualitative in nature, and the tests are just looking for a pass-fail criterion. This does not allow for the application of the collected data to then be applied to other fire scenarios. A well-defined description of the selected materials flammability is not accomplished using just these test methods.

Discussion of the initial evolution of the of the modelling process was compiled by A.P Mouritz and A. G. Gibson in their textbook "Fire Properties of Polymer Composite Materials" [24]. Chapter five within the text specifically discusses the modelling process of composites in fire. It should be noted that when using the term "model" it is commonly used in two contexts; one to define a solver for the conservation equations defining pyrolysis, while also being used to describe a set of parameters that define a material. The text focuses on the use of mathematical models to help describe the heat conduction and fire reaction of composite materials. The heat conduction was most commonly defined as a one-dimensional process where the slab is assumed to heat up with a uniform in-plane temperature distribution. The 1D heat transfer analysis was effective and was used in a multitude of other models [24], however when considering a localized surface heating of a composite a multi-dimensional analysis must be considered. The 3D heat transfer analysis was utilized by a multitude of studies to predict heat transfer. Both the 1D and 3D assumed that the density, specific heat, and thermal conductivity were independent of temperature. The 1D and 3D models did not consider the thermally activated processes that may occur within the composite, this would include such things as the

resin decomposition and the convective flow of volatiles [24]. The heat transfer analysis therefore was defined to work best for composites exposed to low heat fluxes. The final implementation of the heat transfer model was the development and implementation of convection and radiation equations to account for their influences on the heat transfer process. These considerations helped improve the modelling of low heat flux numerical models, defined as 8 to 19 kW m-2.

The developed models from the text all looked to create models for glass matrix composites and were done so in one to two different fire scenarios. Pering, Farrell and Springer [24] developed a model that predicted the thermal response of composites that considered the decomposition of the polymer matrix. Energy transfer by convection was considered negligible and the gases were considered to leave the solid immediately, so they did not affect the temperature. The resultant model showed good agreement with the experimental mass loss rate. A model was then created by Henderson, which proved to be more intricate than Pearson's [25]. Henderson's model considered heat conduction, thermal decomposition and included a new mechanism of the diffusion of decomposition gases. The heat transfer was conducted in 1D however the thermal conductivity was considered to be temperature dependent and was determined experimentally. The mass loss rate was determined using the Arrhenius kinetic rate equation. When compared against experimental data the model performed very well, these tests were performed at high heat fluxes to assure decomposition of the glass/phenolic composites.

A simplified version of the model developed by Henderson was implemented by Gibson, the simplification was in the assumption that the glass-char reactions do

not occur. This would allow the model to become applicable for heat fluxes below 125 kW m-2. Another assumption made were the thermal and gas properties for transport were constant during the decomposition of the material. This model proved accurate for many glass composites at lower heat fluxes when used to predict mass loss rate, time to ignition, and char formation [24]. A model developed by Florio and Henderson was based off of Henderson's original model, but with the inclusion of thermal expansion and pressure rise within the composite. Florio's model did not show any significant improvement in terms of predicting the temperature rise within the composite, then the original model created by Henderson.

The models gone over within the text of A.P Mouritz and A.G Gibson [24] provided an insight into the evolution of the modelling process and provided insight into how these models were developed. It showed that the added complexity to a model does not necessarily yield better results. The models discussed were all for a particular type of composite, glass fibers with a phenolic resin, and tested in very specific fire scenarios, limiting their potential universal usage. This is confirmed in a later journal entry by A.P Mourit et al. [26], where it is again noted that the models used to predict non-reactive fiber composites, fiberglass composites, are robust and can predict temperature rise accurately, but reactive fiber models are still lacking.

The study performed by Javier Trelles and Brian Lattimer [27] compared the results of an Arrhenius-type model to that of a density-temperature relationship model for the transient thermal degradation of a composite. The results of the models were compared to results from a previous study conducted by Boyer [28]. Both models were based of a one-dimensional assumption for the heat transfer through the

composite. The equations used within both of the models within the study resulted in a system of ordinary differential equations (ODEs) and a system of differential-algebraic equations (DAEs) for the Arrhenius and density-temperature methods respectfully. The systems of equations were inputted into Nonmonotonic Nonlinear Equation Solver (NNES) and the piecewise Hermite interpolatory-splines package (PCHIP) for the ODEs and DAEs respectfully. PCHIP was also implemented to determine the temperature dependence of density for the second modeling method. These were then implemented into FORTRAN 95 and resulted in an executable that modeled the composite. The models showed a good fit with the experimental data, and when compared the density-temperature relationship model performed just as well as the Arrhenius model. The results from this study does show other methods for modeling other than the Arrenhius model. The temperature density method discussed within this study allowed for the bypassing of the Arrenhius kinetics determination for the material of interest. The models discussed within the study showed promise in terms of predicting a well-defined 1D heat transfer through a composite material, however with no comparison to mass loss rate (MLR) it is hard to determine if the chemical kinetics were accurately captured. It is also noted that the model was not compared with other materials to see how well it would work with other composite materials.

A study performed by Quintiere et al [29] done for the FAA focused solely on the carbon composite materials and looked to fully characterize the flammability of a material while also providing MLR, mass fraction, heat flow and time to ignition models for the carbon fiber composite. The carbon composite material is a material

fabricated to Boeing material specifications (BMS) 8-276 by Toray Composites [29]. The study also expanded on the bench scale testing previously discussed within the FAA's handbook [22]. These tests looked to examine the ignition time, burning rate and flame spread rate/direction of the fire. The data from these tests were more quantifiable and the ignition time were backed by ignition theory, the issue being that the model could replicate thermally thick conditions well but was to be desired when it came to thermally thin situations [29]. The study utilized milligram scale testing in the form of Microscale Combustion Calorimetry (MCC), Differential Scanning Calorimetry (DSC), and Thermogravetric Analysis (TGA). DSC testing was used to find the specific heat for the material and the heat of decomposition of the material allowing for an understanding of the relationship of how much energy is needed to raise the internal temperature of the sample, as well as the heat produced from the sample as it decomposes. The MCC was utilized to determine the complete heat of combustion for the volatiles produced from the material. The TGA was utilized to determine the mass loss behavior of the material and a single reaction model was constructed to define its kinetics [30]. An in-house device was used to measure the thermal conductivity of the composite, however due to the heat loss from the apparatus there was an estimated 50% error [29]. It was recommended that another apparatus be used/developed to better calculate the conductivity of the composite. The study offers a basis of how a composite should be analyzed but provided a simplified model of only one reaction and an incomplete set of pyrolysis parameters that had not been fully validated against experimental data.

A study conducted by M. T. McGurn, P. Desjardin, and A Dodd [31] utilized the thermal, transport, and kinetic properties for the carbon epoxy composite tested by Quintere et al [29] to help further develop a model for carbon epoxy composites. The model developed by McGurn et al [29] placed a big emphasis on the volumetric swelling model that was implemented within the study. This is held as an important feature due to the fact that the swelling of the composite was shown to have a large effect on the burnout times of the composites. The model was validated against TGA tests run with the sample as well as one sided heating experiments. It was determined from these model validation tests that there was a good agreement and the inclusion of a finite element expansion algorithm led to much better predictions and without out it the model underpredicted results when compared to the experimental tests results. There was no use of DSC results to help determine specific heat capacities of the components, and it was assumed a one reaction model. The Model in this study was only compared against Quintiere's findings [29] and no further testing on other epoxy composites were conducted to validate the model.

A direct follow up study to Quintiere et al [29] was performed by McKinnon et al [32] where the same carbon composite material was re-characterized in terms of its flammability. The main improvement of this study was the use of the Controlled Atmospheric Pyrolysis Apparatus (CAPA) to determine the temporally resolved thermal conductivity of the material rather than the in-house method Quintiere used [29], while also parameterizing the material in more than one dimension. Due to this ThermaKin2D [33] was utilized to perform the necessary calculations to help determine the model characteristics by iteratively changing the values inputted into

the model until a satisfactory agreement had been met to the experimental data. The use of the simultaneous thermal analysis method to perform TGA and DSC was used to provide more concise and accurate results then performing the two on separate apparatuses, especially for the DSC [32]. This was due to the DSC device used by Quintiere being a power compensation type of DSC [34]. The TGA mass loss rate data was modeled using four separate reactions instead of one reaction, where the first three reactions were considered first order reactions with the last being a second order reaction [32]. The study also showed that the oxygen concentration surrounding the back of the sample when in the CAPA did not have any large effects on the data collected. The study showed vast improvement to the previous work [29], while also confirming questions of the environment a sample is exposed to within the CAPA and how that may affect the collected data.

Due to the general nature of composites flammability there has been a drive for research involving their improvement through modifications of the structure and composition of composites. The study performed by Kandola and Kandare [35] looked at the various methods that can be utilized to improve upon a PMC's flammability characteristics. Surface coatings, additive and reactive fire retardants, resin modifications, co-curing of different resins, and nanoparticle inclusion in resin and fiber are all discussed in detail of their advantages for their use in a PMC to better improve its flammability characteristics. It was noted that the most efficient way to protect any material, let alone PMC, would be to implement a fire-retardant coating [35]. The two coatings that were compared within the study were intumescent and ceramic coatings, where the intumescent coatings worked best with a vinyl ester and

phenolic composites, the ceramic coatings worked best for epoxy composites [35]. It was highlighted that the idea of coating, let alone any modification to a PMC, is done with the application in mind, a certain method or coating may work well in one setting while fail in another. The study still remarked that the application of coating to protect materials is the way forward, as well as the development of mathematical models that can be utilized to allow for faster predictions of how materials will behave under prescribed loads and well-defined conditions.

From previous works it is apparent the understanding of composite materials and development of models to represent their flammability in fires has progressed considerably. The shortcomings of the previous works mainly stem from the fact that the models were developed to represent a certain fire scenario, and most models were developed specifically for glass matrix composites with less modelling pertaining to carbon fiber composites. The base composite analyzed within this study, a composite made from graphite fiber and bismaleimide resin made to the specification of LMA MB001 More specifically there has been no work done for the carbon fiber composite specifically analyzed within this study, as well as the protective coatings analyzed within this study.

1.3 Overview

Within this study four different composite materials were characterized in terms of their pyrolysis mechanisms/behavior. The base composite is composed of a hexcel IM7 graphite fiber in a crowfoot satin weave with a Cytec 5250-4 bismaleimide matrix (BMI). The base PMC was prioritized in being the first of the four materials to have a complete detailed pyrolysis model. This was to ensure that

the second portion of the study, exploring the effectiveness of the composite barrier coatings, was not compromised by lack of detail in the base composite.

The exploration of the effectiveness of the composite barrier coatings was done so to try and improve the response of the base composite when exposed to fire. This process required both experiments, to provide the relevant properties and define the chemical processes occurring within the composite, and modelling to determine the response of the combined base composite and barrier coating in fire scenarios. The methodology used to achieve this was that developed by Mark McKinnon, Jing Li and Stanislav Stoliorov [28,34]. This was all done because achieving this comparison using full-scale tests would consume a vast amount of material, something the current lab production would not be able to supply. The process used within this study allows for the exploration of the composites and composite barrier coatings on an experimental scale, something the current production allows for.

Chapter 2: Experimental

2.1 Materials

Within this study four different composite materials were tested that were provided by NAVAIR and manufactured by the NAVAL Air Warfare Centers at China Lake and Patuxent River. The materials consisted of the base composite and three different barrier coatings. The materials were tested individually for the milligram scale testing, they were ground into a fine powder using a SPEX 6775 Freezer/Mill Cryogenic Grinder. For bench scale testing the materials were cut into 0.07 m diameter disks to be used within the CAPA II apparatus.

2.1.1 BMI

BMI is the base composite that is looking to be improved by the application of the barrier composite coatings. The BMI is comprised of IM7 graphite fiber in a crowfoot satin weave (style 1) produced by Hexcel. The matrix material is Cytec 5250-4 bismaleimide matrix. The resin content is 38 ± 2% by weight. The layup of the composite was 24 ply with an quasi-isotropic layup. For the layup the orientation of the fibers was rotated 45 degrees from the previous layers orientation (0,+45,90,-45)3s with an nominal thickness of 4.6 mm. For further details of the manufacturing of the BMI composite please refer to appendix section A.1.

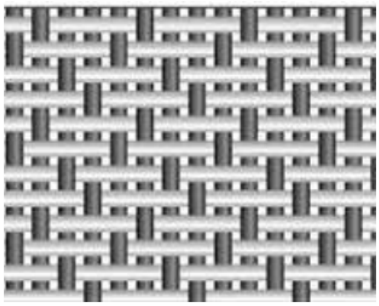

Figure 2.1: Example of a crowfoot satin weave as used in BMI

2.1.2 Composite Barrier Coatings

The Res V barrier coating was comprised of Astroquartz III in a style 4503 plain weave and produced by JPS Composite Materials. The two different resins were used, PT30 cyanate ester produced by Lonza and Cis-resveratrol cyanate ester (Cis-ResVCy) developed by the Naval Air War Center – Weapons Division (NAWCWD). The composition of the resins was 30% PT30 and 70% Cis-ResVcy. The Res V composite coatings was laid up in 4 plies with a nominal thickness of 0.41 mm and the layer orientation was (0,90) on top of the BMI.

The composite barrier coating of Graphite CE is composed of a graphite fiber material called HexTow IM7 produced by Hexcel. The resin selected for the composite was PT30 cyanate ester produced by Lonza. The composite coating was laid up in 2 plies for a nominal thickness of 0.64 mm with a layer orientation of (0,90).

The composite barrier coating of Astroquartz CE is composed of the quartz fiber Astroquartz III in a style 4503 plain weave produced by JPS Composite Materials. The resin used is the same as the Graphite CE, being PT30 cyanate ester produced by Lonza. The composite coating was laid up in 4 plies with a nominal thickness of 0.46 mm with a layer orientation of (0,90).

The details of the composite barrier coatings are summarized in table 2.1, it should be noted that the resin content for all of the barrier coatings was manufactured to have a resin content of roughly 40%, a value provided by NAVAIR.

Table 2.1: Composite Barrier Coatings Compositions and layup details

Fiber	Resin	Plys	Nominal Thickness (mm)	Abbreviation
Astroquartz III	30% Lonza PT30 70% Cis-resveratrol cyanate ester	4	0.41	Res V
Hexcel IM7 graphite	Lonza PT30 cyanate ester	2	0.64	Graphite CE
Astroquartz III	Lonza PT30 cyanate ester	4	0.46	Astroquartz CE

2.2 Milligram Scale Experiments

2.2.1 Simultaneous Thermal Analysis

Simultaneous Thermal Analysis (STA) is a testing method that simultaneously performs Thermogravimetric Analysis (TGA) and Differential Scanning Calorimetry (DSC). This allows for an understanding of the kinetics and thermodynamic properties of a thermally thin material. This is achieved with two symmetrical crucibles placed within the apparatus with one crucible being kept empty and the other holding the material of interest. A prescribed temperature program is then applied to the crucibles and the heat flow and mass evolution are measured with two thermocouples beneath each crucible and a high sensitivity mass balance. Both the heat flow data and mass data are recorded with respect to time and temperature. Within this study a Netzsch STA 449 F3 Jupiter was used to perform all of the STA testing. It was calibrated in accordance with the user manual using well-defined standard samples.

A baseline correction test was run prior to each sample test, where both crucibles are empty and run through the same heating program that would be used for the sample test. This is performed to allow for correction of differences in environment, buoyancy effects, and the asymmetry of the furnace and sample crucibles. The tests were performed in an anaerobic environment, which was maintained by a constant flow of nitrogen. This was done to emulate the anaerobic pyrolysis conditions that occur within a diffusion flame. Powdered samples were packed tightly into the sample crucible to allow for maximum thermal contact and heat flow sensitivity. A lid with a small hole was placed on both crucibles to allow for the gaseous products from the sample to exit the crucible.

Each composite was tested 10 - 13 times, with the powdered samples varying between 4 - 6 mg between tests. The samples were brought to a steady temperature of 313 K for 10 minutes before beginning a temperature program of 10 k min^{-1} until reaching a furnace temperature of 1173 K. The nitrogen flow rate was held at a constant 50 ml min^{-1}.

2.2.2 Microscale Combustion Calorimetry

Milligram samples, between 8.8 – 9.4 mg and considered thermally thin, were placed in an open-top ceramic crucible then raised and sealed within the pyrolyzer of the MCC. Within the pyrolyzer of the MCC an anaerobic environment was kept with a constant flow of nitrogen at 80 ml min^{-1}. The sample was then raised to steady temperature of 348 K before a nominal heating rate of 60 K min^{-1} was applied. As the pyrolyzate gases are formed they move to the combustor where they were introduced and mixed in an environment of excess oxygen, introduced at a rate of 20 ml min^{-1}.

The pyrolyzate gases, now mixed with oxygen are then fully combusted within the combustor. The combustor was maintained at a temperature of 1203 K to allow for the complete combustion of the pyrolyzate gases. Heat release rate data was captured as a function of temperature and time using the principals of analytical pyrolysis, combustion gas analysis by oxygen consumption, and pyrolysis combustion flow calorimetry. More detailed literature on the MCC is available [36].

As stated previously all the MCC was conducted in open ceramic crucibles that allowed for the easy escape of the pyrolyzate gases that formed during the experiment. Each test was performed carefully to ensure that the mass of the material was recorded both before and after the test to allow for the calculations of the char yield and total mass consumed during the testing. Each of the four materials was tested three times due to the high reproducibility of the results.

The MCC's temperature and oxygen sensors were calibrated to allow for accurate results. The temperature sensors within the MCC were calibrated using known pure metals, and their well-defined melting point temperatures. The oxygen sensor was calibrated using a well-defined oxygen/nitrogen mixture to obtain accurate oxygen consumption measurements.

2.3 CAPA II Testing

For the bench scale experiments each sample was not tested individually as they were in the milligram scale experiments. BMI was tested on its own while the other samples tested involved the base composite of BMI with a composite barrier coating applied to the top surface in the thicknesses as described in table 2.1. The samples were uniformly all cut to 7 cm diameter disks and prepared in the same

manner. Each sample had a thin disk of copper foil adhered to the back of the sample with a high temperature epoxy. The copper was then painted with a high emissivity paint, an emissivity value of 0.92, and cured and stored within a desiccator for at least 24 hours before testing.

Each sample was prepared in the same manner before each test; The samples were received initially as a 0.3 by 0.3 meter square plate, where a water jet was then used to cut out 7 cm disks with an average thickness of 4.6 mm. Each sample was then weighed, and their mass recorded before placing a thin layer of epoxy glue, on average 0.3 grams worth, on the back of the sample. The sample was then reweighed with the epoxy and a copper disk 9 cm in diameter and 1.27×10^{-3} meters in thickness was applied to the back of the sample. The sample was then re-weighed and placed within a hood to have a high emissivity paint applied to the surface of the copper. The paint was then cured under a heat gun for 30 minutes and weighed one last time. the sample was then rests in a desiccator for 24 hours before being tested.

2.3.1 Controlled Atmosphere Pyrolysis Apparatus II

The Controlled Atmosphere Pyrolysis Apparatus II is a testing apparatus designed to allow for the analysis of pyrolysis and thermal degradation of non-

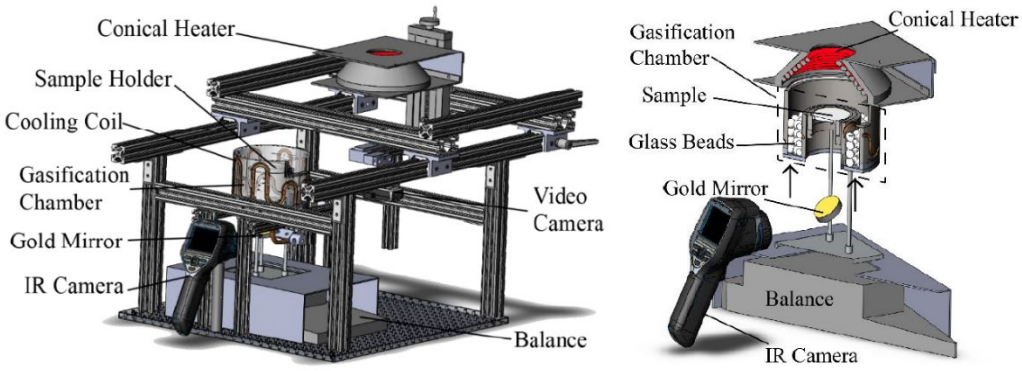

Figure 2.2: Schematic of the controlled atmosphere pyrolysis apparatus II (CAPA II)

thermally-thin samples. The apparatus is displayed in detail within figure 2.3. A sample is prepared in the size of a 7 cm disk and placed in a well-defined and monitored environment, where a prescribed heat flux is then introduced to the sample. The heat flux was measured prior to each test with a calibrated heat flux gauge to measure and verify the heat flux that would be applied to the sample for the duration of the test. The samples mass is then measured over the duration of the test using a high precision balance, while the back temperature of the sample is measured from the reflection of the sample off of a gold plate with a calibrated Infrared (IR) camera for the duration of the test. The IR camera temperatures and mass data are collected with respect to time.

A flow rate of 185 SLPM of nitrogen is used throughout the duration of the test to create an anaerobic environment to simulate the pyrolysis of a diffusion flame. The emissivity of the paint used to coat the back of the copper sheet on each sample is .92 and the IR camera was calibrated every time a new can of high emissivity paint was used to ensure the back temperature readings were accurate for all of the tests performed. Tests were performed at 65 kW m^{-2} for all of the samples with at least two tests being performed for each sample. One set of two tests were performed on the BMI samples with no coating at 85 kW m^{-2} for validation purposes.

Chapter 3: Modeling

All of the modelling performed was done so through ThermaKin 2Ds, a numerical pyrolysis solver used to simulate a given materials exposure to a defined heat source. ThermaKin 2Ds is able to create these models by solving non-steady mass and energy conservation equations based upon the input parameters that are defined by the user for a given material/set of materials. A detailed description of the equations used within ThermaKin and validation can be found in previous works done [18, 37].

ThermaKin 2Ds interprets two user defined files to produce a model of a material(s) of interest. The files are defined as the component file and conditions file. The latter is where the materials being modelled are defined in terms of their chemical kinetics and their properties. These properties entail density, heat capacity, thermal conductivity, emissivity, gas transfer coefficient, and radiation absorption coefficient. These properties are defined for all the virgin materials involved, and will also include all the properties for all of the intermediate phases the material may go through to best represent the chemical and physical phenomena while exposed to the prescribed heating conditions. The conditions file is used to define the heating rate and subsequent boundary conditions, the geometry and position of the materials, and define parameters to set the resolution for the model.

ThermaKin was used as the solver for the models developed within this study, a separate set of scripts written in MATLAB were used to optimize the results from the ThermaKin models to make sure the parameters and properties found through

inverse modelling converged on a meaningful value. The scripts utilized were written by Greg Fiola and are described in detail in his work [38,39].

Chapter 4: Milligram-Scale Experimental and Modelling Results

For all the milligram experiments performed each composite had been ground to a fine powder using a Spex cryomill and tested separately in each apparatus to obtain specific thermal properties for each material. The powders were kept in a desiccator at all times, only being removed for testing. The errors displayed within section 4.1 were calculated as two standard deviations of the mean.

4.1 Milligram-Scale Experimental Results

A comparison of the MLR from the results from the TGA are displayed within figure 4.1. The TGA MLR experimental data shows a general trend for all the data in terms of each achieving its maximum peak MLR around 720 K. The barrier coatings then follow a similar pattern of a visible second reaction with the peaks occurring around 850 K. At the end of the test when the samples have reached 1173 K, all of the samples have reached a similar MLR value of just above zero. This most likely signifies all the reactions are finished if not just about finished within all the samples by the end of the test. The BMI, as expected being the base composite looking to be improved, lost the most amount of mass for the TGA tests. The Res V and Astroquartz CE lost similar amounts of mass, with the Graphite CE losing the least amount of mass. A summary of the results is displayed within table 4.1.

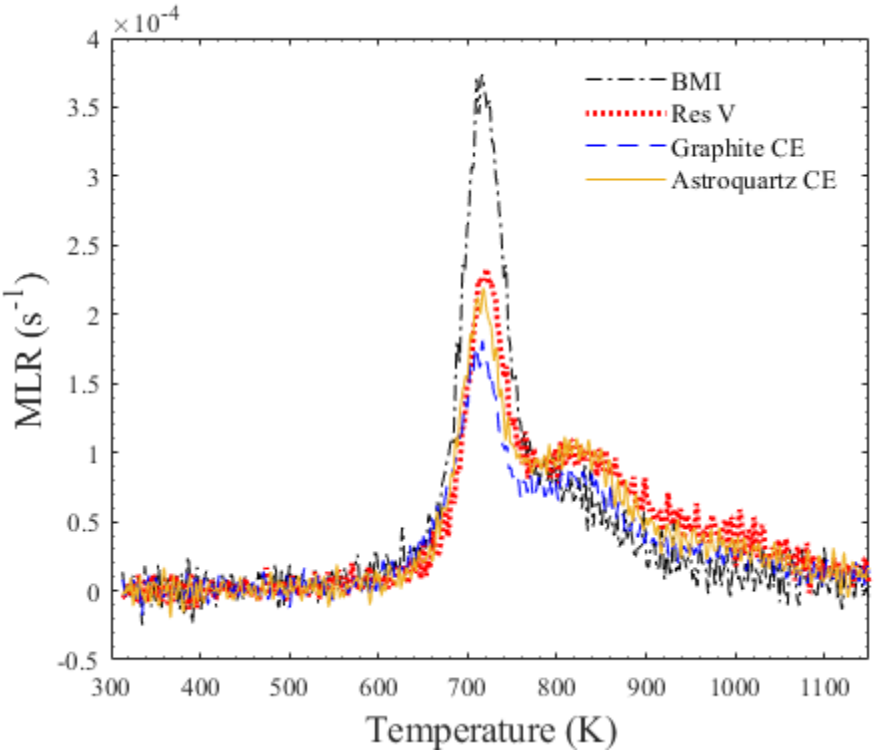

Figure 4.1: Comparison of averaged TGA mass loss rate of all composites. All of the MLR data was smoothed using a three-point average to allow for a clearer distinction between the curves.

Table 4.1: Summary of Average TGA Results

Samples	**Onset of Mass Loss Rate (K)***	**Max Mass Loss Rate (s^{-1})**	**Residue Yield**
BMI	661 ± 7	$(3.85 \pm 0.33) \cdot 10^{-4}$	.766 ± .004
Res V	676 ± 2	$(2.34 \pm 0.15) \cdot 10^{-4}$	.774 ± .002
Graphite CE	665 ± 2	$(1.97 \pm 0.32) \cdot 10^{-4}$	.819 ± .003
Astroquartz CE	671 ± 1	$(2.24 \pm 0.22) \cdot 10^{-4}$	.790 ± .005

** The onset of mass loss rate was determined when the mass loss rate first reached a value of 0.5 x 10^{-4} s^{-1}*

The average DSC heat flow curves are displayed within figure 4.2. For all of the composites the heat flow data follows the same trend until 480 K where the heat flow between all of the composites begin to diverge. All of the composites start off as an endothermic process absorbing heat until the beginning of the first reaction around 620 K where the base composite, BMI, sees a rise in its heat absorption. In contrast the composite barrier coatings drop considerably in heat flow, this is in correspondence with the initial reaction. Both the Res V and Astroquartz CE end up producing heat for a brief period of time, before returning back to absorbing heat for the rest of the test. Table 4.2 reiterates the important details for each of the composites found from the DSC data, where the negative values dictate an exothermic reaction.

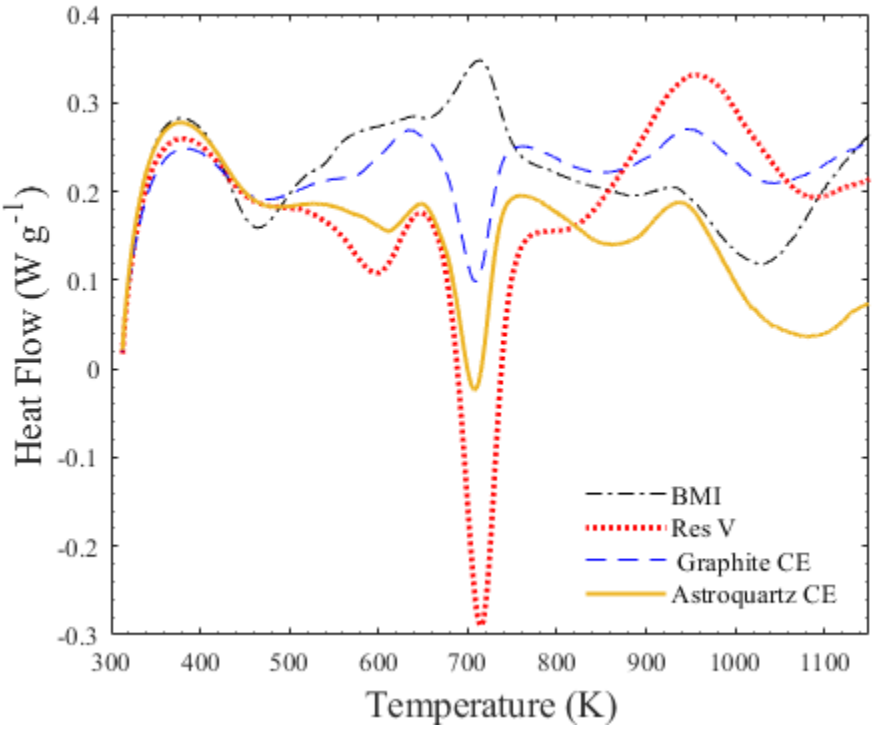

Figure 4.2: Comparison of averaged DSC heat flow of all composites. Each test was normalized by its initial mass before being averaged.

Table 4.2: Summary of Average DSC Results

Samples	Peak Exothermic Heat Flow (W g^{-1})	Temperature at Peak (K)	Integral Heat Flow at 900 K (J g^{-1})
BMI	NA*	NA	821 ± 136
Res V	-0.290 ± 0.031	715 ± 1	485 ± 71
Graphite CE	0.098 ± 0.052	709 ± 1	737 ± 161
Astroquartz CE	-0.017 ± 0.047	708 ± 1	596 ± 125

** The peak exothermic heat flow was determined at the point where the samples, excluding the BMI, minimum peak occurred.*

The HRR data collected from the MCC and displayed in figure 4.3 reiterates the vast difference between the base composite BMI and the three composite barrier coatings. The three barrier coatings all show similar behavior in terms of their HRR, with the onset of HRR first occurring for Graphite CE followed by Astroquartz CE and then finally by the Res V. When looking at the heats of combustion for the composite barrier coatings, the Res V has the lowest value with 2.46 ± 0.13 kJ g^{-1} closely followed by Graphite CE being 2.72 ± 0.30 kJ g^{-1} and finally Astroquartz at 3.35 ± 0.13 kJ g^{-1}. These values as well as others are found in table 3.3. These values are all vast improvements on BMI, however it is worth reiterating that they will be utilized as coatings not as a replacement for BMI so though their HRR and subsequent heat of combustion is less it requires further testing to verify if they would work well as a barrier coating.

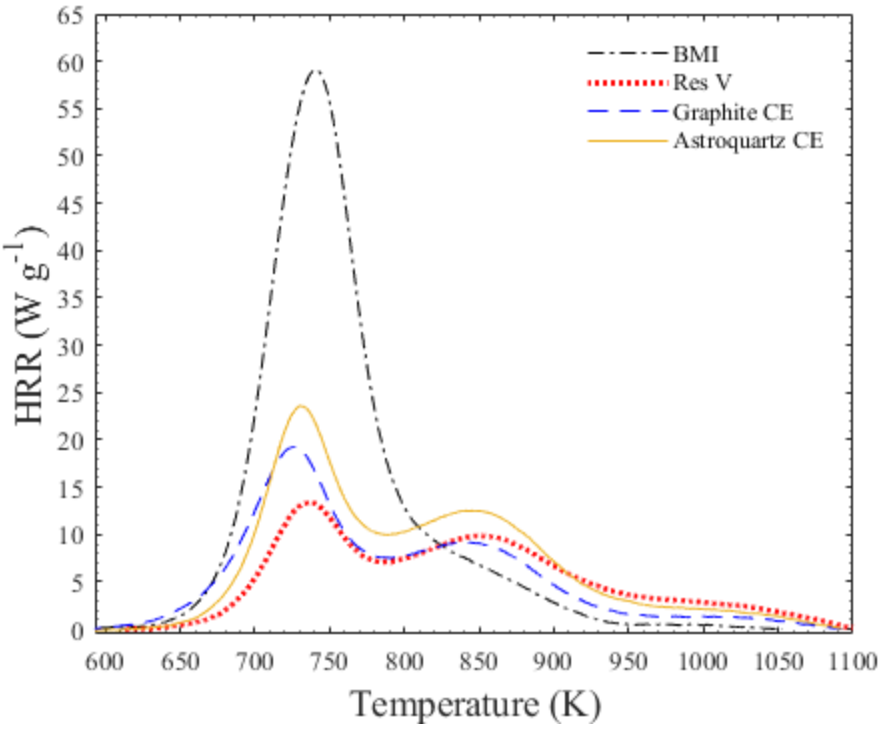

Figure 4.3: Comparison of averaged Normalized Heat Release Rate of all composites. Each test was normalized by its initial mass before being averaged.

Table 4.3: Summary of Average MCC Results

Composites	**Onset of HRR (K)***	**Peak HRR ($W\ g^{-1}$)**	**Residue Yield**	**Heat of Combustion ($kJ\ g^{-1}$)**
BMI	672 ± 4	58.6 ± 2.5	.762 ± .008	5.07 ± 0.15
Res V	698 ± 5	13.3 ± 0.5	.791 ± .011	2.49 ± 0.13
Graphite CE	672 ± 3	19.1 ± 1.0	.835 ± .007	2.72 ± 0.30
Astroquartz CE	685 ± 2	23.3 ± 0.7	.815 ± .016	3.35 ± 0.13

**The onset of HRR was determined when the average HRR value first reached a value of 5 $W\ g^{-1}$*

4.2 Milligram-Scale Modelling Setup and Results

4.2.1 Test Conditions

To emulate the milligram-scale testing of TGA, DSC, and MCC the conditions file was set to work in a single dimension under the assumption of a thermally thin sample. The mass transport of the gas was set so that the gases leaving the sample faced no resistance. The heating of the sample was constructed with a high convective coefficient of 1×10^5 W m^{-2} K^{-1} at the boundary of the sample to simulate the material heating at the same temperature as its prescribed surroundings. The heating rate prescribed for the model was determined from the average heating of all the STA experiments and MCC experiments, respectively. This was done by fitting a decaying sinusoid function to the experimental heating rate, *dT/dt*, with respect to time, *t*, described in equation 4.1.

$$\frac{dT}{dt} = 60\frac{sec}{min} \times \exp(-bt) \times [\cos(ft) + g\sin(ft)] \qquad (4.1)$$

Using equation 4.1 the nominal heating rate of 10 K min^{-1} and 60 K min^{-1} were modelled for the STA and MCC tests respectively. The results are displayed within figure 4.4.

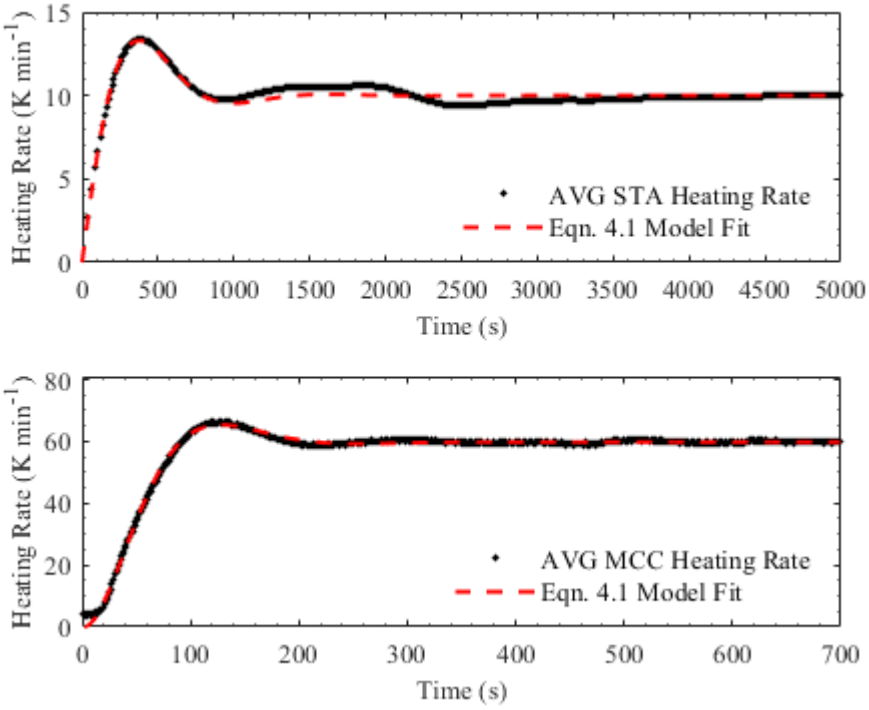

Figure 4.4: Heating rate for both STA and MCC experiments at 10 K min^{-1} and 60 K min^{-1} respectively.

The heating rate coefficients for equation 4.1 are defined in table 4.4 for both the STA experiments conducted at 10 K min^{-1} and the MCC experiments conducted at 60 K min^{-1}. For all of the milligram scale models the time step was set to 0.001.

Table 4.4: Equation 4.1 Heating rate coefficients

Heating Rate	a ($K\ s^{-1}$)	b (s^{-1})	f (s^{-1})	g
STA (10 K min-1)	0.1667	0.003081	0.005097	-0.7870
MCC (60 K min-1)	0.9950	0.01860	-0.02476	-0.7991

4.2.2 Milligram-Scale Modelling Results

The modelling results for the milligram scale testing were performed in the order of TGA, DSC and finally MCC data. The modelling was performed to determine properties for each of the composites individually by performing inverse analysis on the averaged milligram-scale experimental data. Models were first constructed for the TGA data set to determine the number of reactions, their order, and kinetic coefficients along with the corresponding stoichiometric coefficients. The reaction mechanisms and kinetics determined from the inverse analysis of the TGA data for each composite was then used within the corresponding DSC and MCC analyses. The DSC analysis was then performed to determine the heats of reaction and heat capacities for each of the composites. The MCC analysis was performed to determine the heat of combustion for the gases from each reaction occurring in each composite. The results of the inverse analysis and the corresponding models for each composite are performed within this section beginning with the base composite BMI displayed in figure 4.5. The error bars within figure 4.5 were calculated as two standard deviations of the mean.

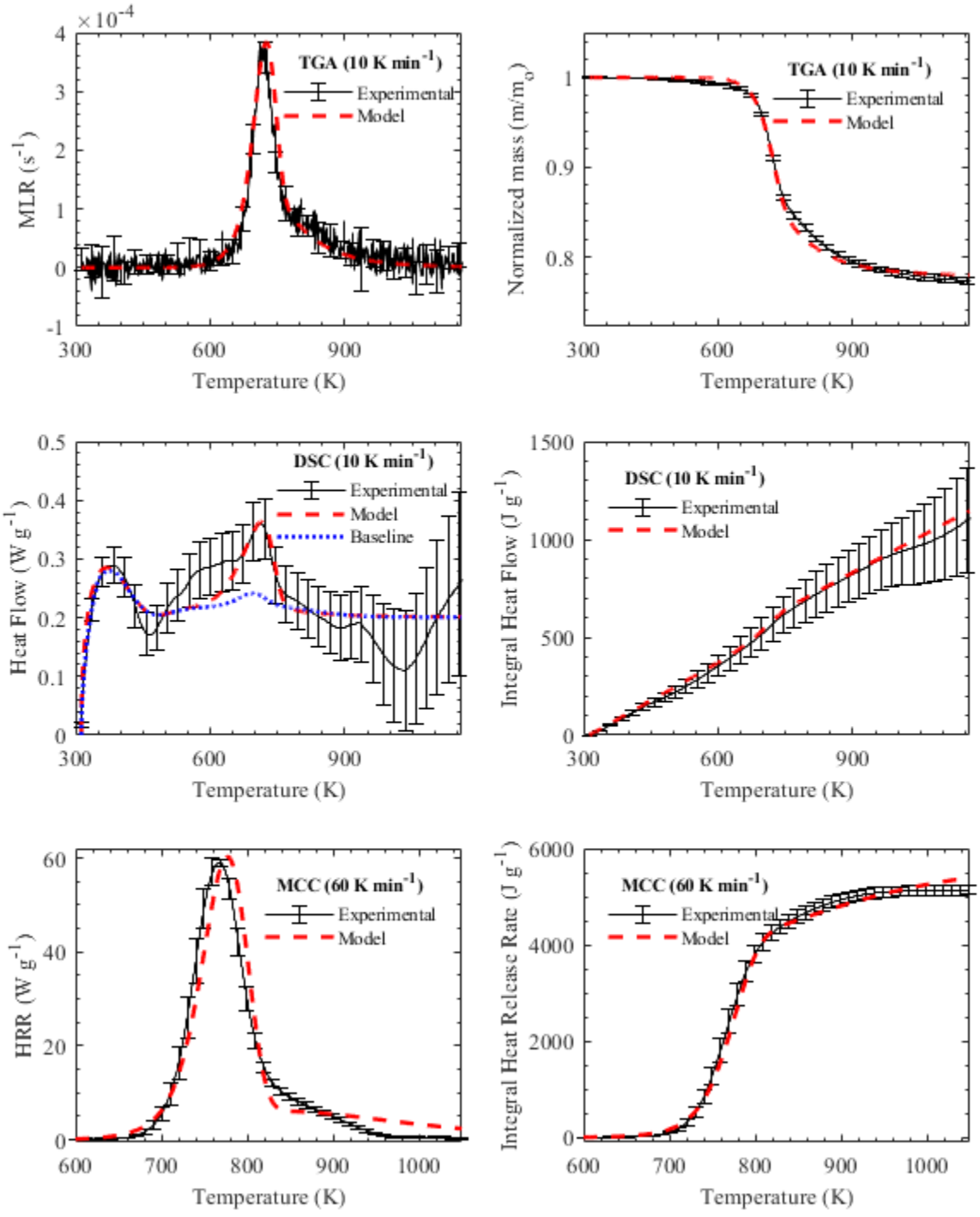

Figure 4.5: Averaged Milligram-scale testing for BMI compared to ThermaKin modeling.

The TGA inverse analysis for BMI resulted in a three-reaction model representing the BMI where the first reactions were considered first-order reactions with the third and final reaction being a second order reaction. The second order reaction was implemented to better predict the HRR of the MCC, as with a first order reaction the production of gas from the 2nd intermediate was too slow. The reaction scheme for BMI is displayed within Table 4.5.

Table 4.5: Reaction Model for BMI developed from TGA Experiments

i	**Reaction**
1	$BMI \rightarrow \Theta_1 BMI_{int\ 1} + (1-\Theta_1) BMI_{gas\ 1}$
2	$BMI_{int\ 1} \rightarrow \Theta_2 BMI_{int\ 2} + (1-\Theta_2) BMI_{gas\ 2}$
3	$(0.5) BMI_{int\ 2} + (0.5) BMI_{int\ 2} \rightarrow \Theta_3 BMI_{char} + (1-\Theta_3) BMI_{gas\ 3}$

The reaction model developed was then used to perform an inverse analysis on the TGA BMI data to find the activation energy (E) and Arrhenius constant (A) used within the reaction rate equation and the stoichiometric coefficients (Θ_i). The MLR for the TGA experiments was captured well, only just slightly over predicting the residue yield when compared to the experimental data.

Once the TGA had been properly modelled the DSC experimental data was then inversely analyzed to determine a baseline heat flow to define the heat capacities for each solid component within the reaction. The heat capacities (c) for BMI are displayed within Table 4.6.

Table 4.6: Summary of BMI component heat capacities

Component	c (J kg^{-1} K^{-1})	Temperature Range (K)
BMI	-3370 + 13.4T	$T \leq 341$
	113.1 + 3.1T	$341 < T \leq 368$
	814.6 + 1.2T	$368 < T \leq 394$
	1550	$394 < T$
$BMI_{int\ 1}$	1550	$394 < T$
$BMI_{int\ 2}$		
BMI_{char}		
$BMI_{gas\ 1}$	2100	$394 < T$
$BMI_{gas\ 2}$		
$BMI_{gas\ 3}$		

The gas components defined in the reaction model defined in table 4.5 for BMI were held at a constant heat capacity of 2100 J kg^{-1} K^{-1}, as defined in table 4.6, corresponding to the mean heat capacities of a gaseous C1 – C8 hydrocarbons at 600K [40].

Once the baseline had been defined, the heats of reaction (h) were then manually adjusted until the model heat flow curve best fit the experimental data. Fitting the model after 900K was not attempted due to the great divergence of the data after 900K. This can be seen by the noticeable increase in the error bars length. The divergence of data after 900K is most likely also influenced by the loss of sensitivity of the DSC at higher temperatures. The summary of the reaction stoichiometry, kinetics, and thermodynamics is provided in table 4.7.

Table 4.7: Summary of BMI reaction stoichiometry, kinetics, and thermodynamics. Negative heat of reaction indicates exothermic reaction

Reaction #	A_i (s^{-1})	E_i (kJ mol^{-1})	h_i (J kg^{-1})	Θ_i
1	$1.85 \cdot 10^6$	110	$-2.3 \cdot 10^4$	0.981
2	$7.87 \cdot 10^8$	153	$-4.3 \cdot 10^4$	0.876
3	3.49	52	0	0.905

The experimental data for the MCC was shifted to the right by adding 27K to collected experimental temperature data. The MCC data was then analyzed to determine the heats of combustion for each of the gases produced from the three reactions taking place for BMI. These values were manually adjusted until a satisfactory agreement between the model and experimental data was found. The Integral of HRR curve was better suited to determine how well the model captured the experimental data. It was determined that the heats of combustion for the gases produced were 20 kJ g^{-1}, 31 kJ g^{-1}, and 20 kJ g^{-1} for BMI_{gas1}, BMI_{gas2} and BMI_{gas3} respectively. The process of assessing the composite barrier coatings was performed in the same manner as the BMI. The results for each composite barrier coating can be seen in figures 4.6 - 4.8. The error bars within figure 4.6 – 4.8 were calculated as two standard deviations of the mean.

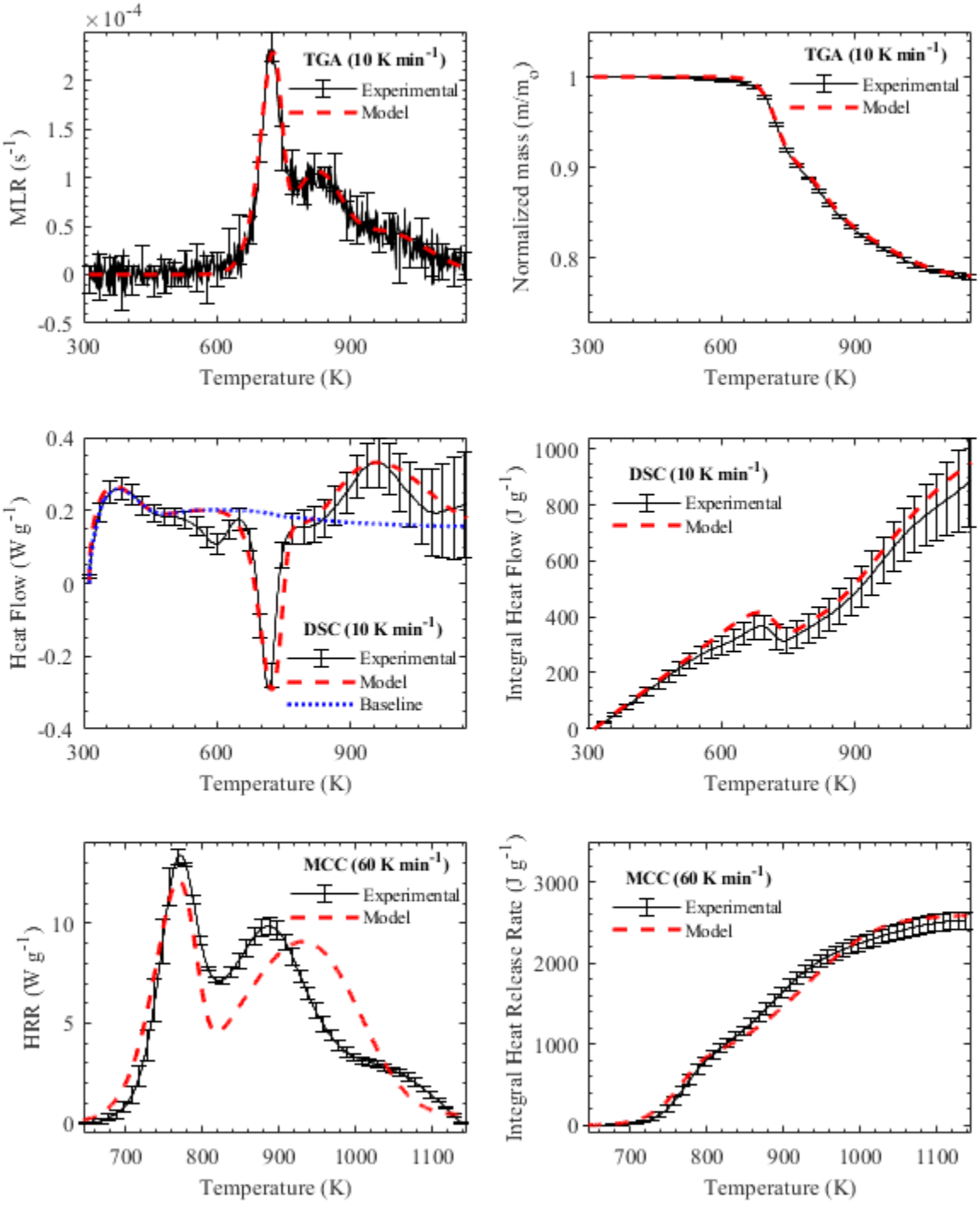

Figure 4.6: Average Milligram-scale testing for Res V compared to ThermaKin modelling.

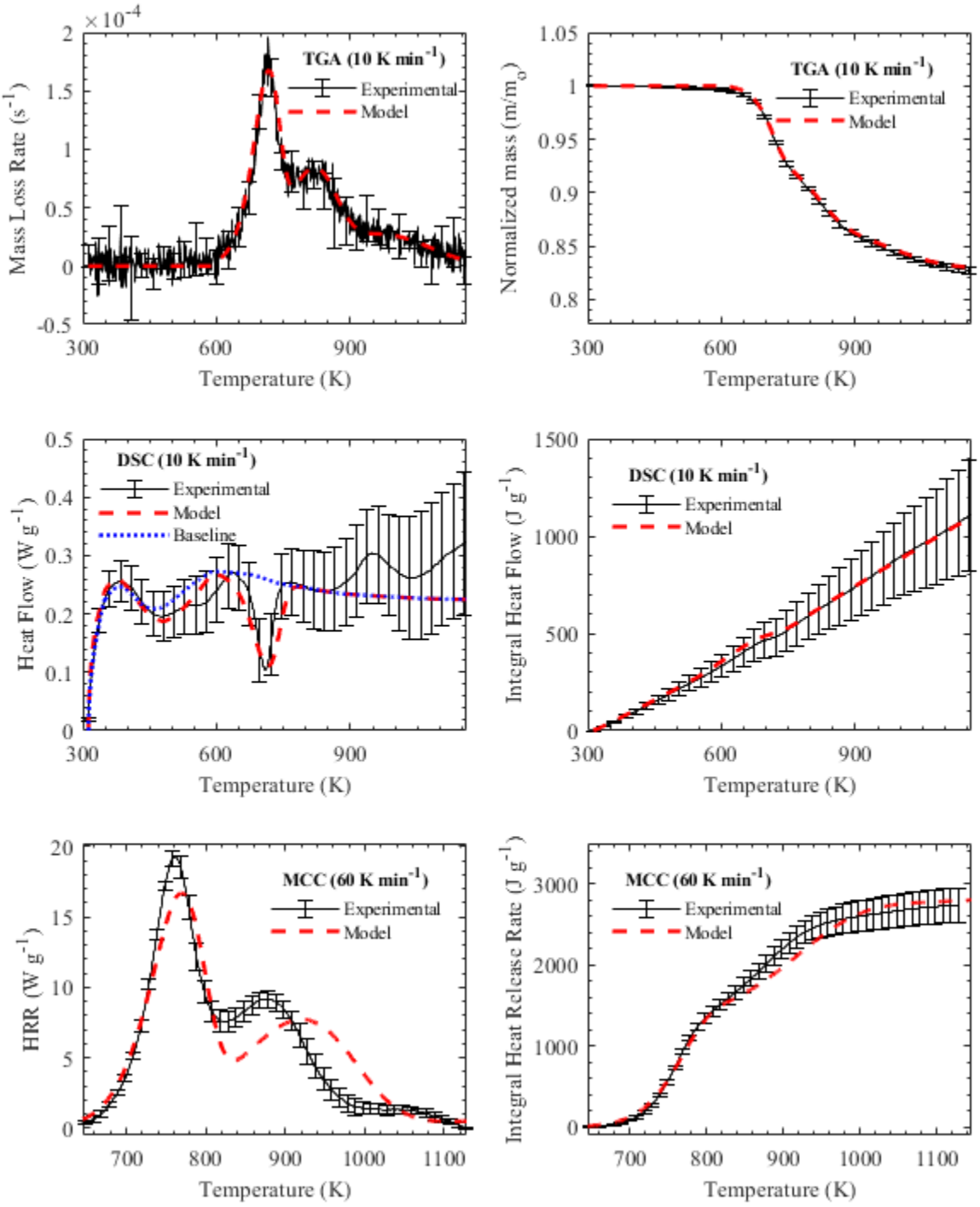

Figure 4.7: Average Milligram-scale testing for Graphite CE compared to ThermaKin modelling.

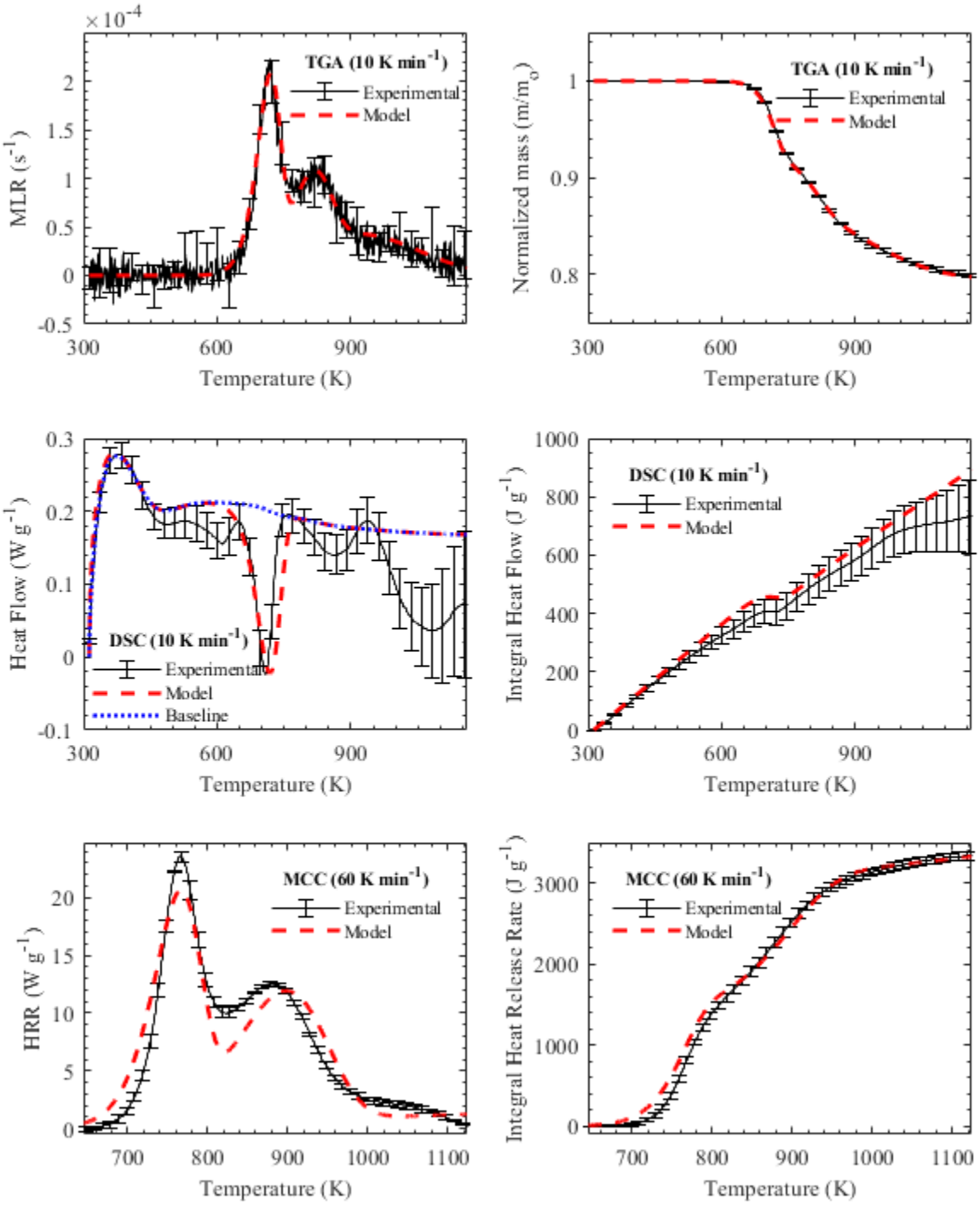

Figure 4.8: Average Milligram-scale testing for Astroquartz CE compared to ThermaKin modelling.

For all of the composite barrier coatings the reaction scheme was the same for each. Each composite barrier coating was found to have three first order reactions. The reaction scheme is displayed in table 4.8. This reaction scheme allowed for a good fit when comparing the constructed models to the MLR and mass fraction of the composite barrier coatings. The subsuqent stoichemometry and kinetics were then determined through the automated optimization, and the DSC data was manually analyzed to determine the heats of reactions. All of these properties are displayed within table 4.9.

Table 4.8: Reaction model for all Composite Barrier Coatings (CBC)

i	**Reaction**
1	$CBC \rightarrow \Theta_1 CBC_{int\_1} + (1-\Theta_1)CBC_{gas\_1}$
2	$CBC_{int\_1} \rightarrow \Theta_2 CBC_{int\_2} + (1-\Theta_2)CBC_{gas\_2}$
3	$CBC_{int\_2} \rightarrow \Theta_3 CBC_{char} + (1-\Theta_3)CBC_{gas\_3}$

Table 4.9: Summary of CBC reaction stoichiometry, kinetics, and thermodynamics. Positive heat of reaction indicates endothermic reaction.

CBC	**Reaction #**	**A_i (s^{-1})**	**E_i (kJ mol^{-1})**	**h_i (J kg^{-1})**	**Θ_i**
Res V	1	$3.05 \cdot 10^{10}$	175	$1.8 \cdot 10^5$	0.923
	2	$4.80 \cdot 10^2$	82	$3.6 \cdot 10^4$	0.916
	3	1.91	58	$-2.9 \cdot 10^5$	0.922
Graphite CE	1	$9.54 \cdot 10^7$	140	$6.8 \cdot 10^4$	0.931
	2	$1.51 \cdot 10^3$	89	0	0.934
	3	1.63	57	0	0.953
Astroquartz CE	1	$3.63 \cdot 10^9$	162	$9.0 \cdot 10^4$	0.922
	2	$4.31 \cdot 10^4$	110	0	0.936
	3	0.19	40	0	0.921

The heat capacities were determined to define a baseline for the the composite barrier coatings in terms of their heat flow. All of the composite barrier coatings heat

capacities are defined using piecewise linear relationships with temperature before reaching a steady state value. The intermediate, char, and gas components formed in each reaction were held at constant heat capacity values. The heat capacity relationships are defined in detail within table 4.10.

Table 4.10: Summary of Composite Barrier Coatings heat capacities

Component	c (J kg^{-1} K^{-1})	Temperature Range (K)
Res V	-3370 + 13.4T	$T \leq 341$
	113.1 + 3.1T	$341 < T \leq 368$
	814.6 + 1.2T	$368 < T \leq 394$
	1550	$394 < T$
Res $V_{int\ 1}$	1550	394 < T
Res $V_{int\ 2}$		
Res V_{char}		
Res $V_{gas\ 1}$	2100	$394 < T$
Res $V_{gas\ 2}$		
Res $V_{gas\ 3}$		
Graphite CE	-1484 + 7.3T	$T \leq 351$
	237.2 + 2.3T	$351 < T \leq 387$
	605.9 + 1.4T	$387 < T \leq 423$
	59.9 + 2.7T	$423 < T \leq 590$
	1625	$590 < T$
Graphite $CE_{int\ 1}$	1625	590 < T
Graphite $CE_{int\ 2}$		
Graphite CE_{char}		
Graphite $CE_{gas\ 1}$	2100	590 < T
Graphite $CE_{gas\ 2}$		
Graphite $CE_{gas\ 3}$		
Astroquartz CE	-2723 + 11.5T	$T \leq 341$
	259.6 + 2.7T	$341 < T \leq 368$
	850.0 + 1.1T	$368 < T \leq 395$
	1265	$395 < T$
Astroquartz $CE_{int\ 1}$	1265	395 < T
Astroquartz $CE_{int\ 2}$		
Astroquartz CE_{char}		
Astroquartz $CE_{gas\ 1}$	2100	395 < T
Astroquartz $CE_{gas\ 2}$		
Astroquartz $CE_{gas\ 3}$		

The gas components defined in the reaction model in table 4.8 for the composite barrier coatings were held at a constant heat capacity of 2100 J kg^{-1} K^{-1}, as defined in table 4.10, corresponding to the mean heat capacities of a gaseous C1 – C8 hydrocarbons at 600K [40].

The MCC experimental data was modelled manually for each of the composite barrier coatings with the resultant heats of combustion for each of the reactions displayed in table 4.11.

Table 4.11: Summary of Composite Barrier Coatings heat of combustions for individual gases released from reactions

Component	**Heat of Combusiton (kJ g^{-1})**
Res $V_{gas\ 1}$	10.0
Res $V_{gas\ 2}$	22.5
Res $V_{gas\ 3}$	2.5
Graphite $CE_{gas\ 1}$	20
Graphite $CE_{gas\ 2}$	22.0
Graphite $CE_{gas\ 3}$	5.0
Astroquartz $CE_{gas\ 1}$	19.0
Astroquartz $CE_{gas\ 2}$	27.5
Astroquartz $CE_{gas\ 3}$	10.0

The inverse analysis performed for the base composite, BMI, and all the composite barrier coatings; ResV, Graphite CE and Astroquartz CE, was able to provide models as seen within the figures of this chapter that provided an accurate representation of the experimental data. This gives confidence in the material properties derived from the inverse analysis and the further testing performed on the CAPA II to fully resolve the material properties of all the composites and further

determine if and what barrier coating provides the best improvement to the base composite of BMI.

Chapter 5: CAPA II Experimental and Modelling results

5.1 CAPA II Experimental Results

The testing performed on the CAPA II consisted of testing the base composite BMI at 65kW m^{-2} and 85kW m^{-2}. Testing performed at 65kW m^{-2} provided more resolved back surface temperature results when compared to the results performed at 85kW m^{-2}. For this reason the composite barrier coatings tests were all conducted at 65kW m^{-2} only. The collected data was recorded at different frequencies. The data for corresponding samples were then binned and then averaged to account for this. Every 11 data points, corresponding to roughly 5 seconds of elapsed time, were then binned, and averaged across corresponding binned data. The data displayed for the MLR and back temperature within this section is all averaged binned data.

It was found through all the tests run on the CAPA II that there was an initial mass loss rate occurring from the samples that could be accounted for by the kaowool insulation used to hold the sample in place. To compensate for this a baseline was constructed and subtracted from each individual binned MLR data set. The baselines were validated accurately taking in account the kaowool MLR, as the new adjusted final mass increased by the same amount of mass lost when kaowool was tested by itself at the same heat flux. The baseline and subsequent adjusted MLR and mass fraction is shown for a single BMI test, test 9, in figure 5.1 (a) as an example for what was performed for all of the experimental MLR data collected from the CAPA II. The baseline was constructed by averaging the first 25 seconds of data when the MLR should be on average very close to zero. This value was then taken, and a linear line was constructed from the 25 point average value to 0 from the beginning of the test to

the point of which the MLR was deemed to cease any drastic fluctuations. For the 65 kW m^{-2} testing it was found that the point at which the decreasing linear line would reach a value of zero was at 500 seconds, while the point of transition for the 85 kW m^{-2} tests was at 400 seconds. This baseline was then subtracted from the original binned MLR data for each test and was then averaged across like samples.

The mass fraction was recalculated using equation 5.1. The mass loss rate for the capa (MLR_c) is normalized by the area of the sample (A_c) making the units of the MLR_c to be kg s^{-1} m^{-2}. The integral is taken with respect to time yielding the mass of the sample normalized by the area of the sample at any given point during the test. To make this unitless the value is multiplied by A_c and divided by the initial mass of the sample (m_{i_capa}) yielding the percentage of mass lost over the duration. This value is then subtracted from 1 yielding the adjusted mass fraction (MF_c) for the test. The results of this are displayed in figure 5.1 (b).

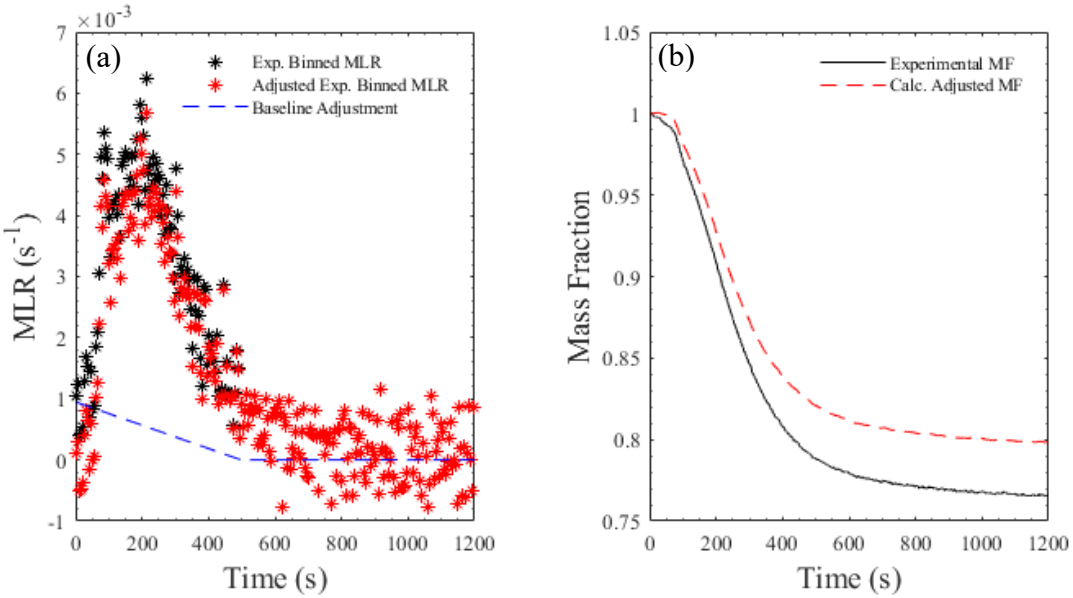

Figure 5.1: Baseline correction for (a) MLR and (b) Mass Fraction CAPA II test on BMI performed at 65 kW m^{-2} of radiant heat flux.

$$MF_C = 1 - \frac{A_c}{m_{i\_capa}} \int_0^t MLR_c \tag{5.1}$$

With the necessary adjustments made and the data binned and averaged for each barrier coating the average MLR for each component was compared in figure 5.2.

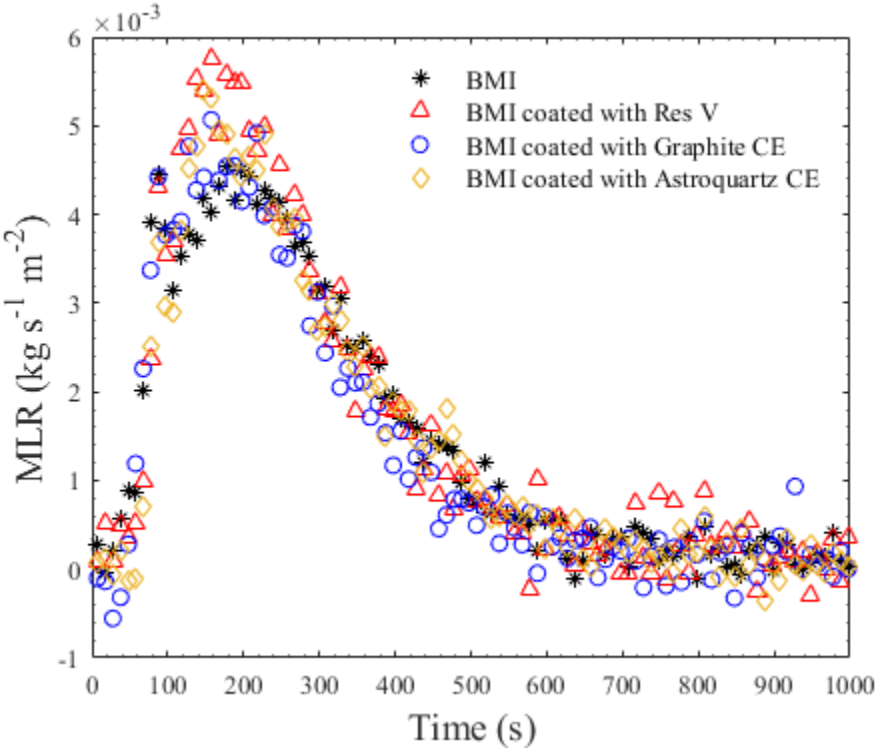

Figure 5.2: Comparison of the CAPA II MLR of base BMI and BMI composites coated with barrier coatings applied at 65 kW m^{-2}.

The MLR for the base composite BMI and the subsequent tests with the barrier coatings as a thin layer on BMI all share a very similar MLR rate profile. The barrier coatings on BMI tend to on average have a slightly higher peak MLR then that of the pure BMI. This would indicate that the current barrier coatings applied to the tops of the BMI at their current thickness did not act as effective gas transport barriers

and compounded with the MLR of the BMI to create a higher peak in the MLR then of just plain BMI. Further examination of the comparison between the BMI and BMI composites coated with barrier coatings is compared in figure 5.3. viewing the back temperature data the profiles for all of the samples are very similar, with the BMI trending lowest until 700s where it transitions to a higher temperature but still staying within 10 K of the lowest temperature profile. Due to the very similar temperature profiles, especially when taking into account the overlaps from uncertainty, for the BMI and BMI coated with barrier coatings it shows the ineffectiveness of the barrier coatings as a thermal barrier.

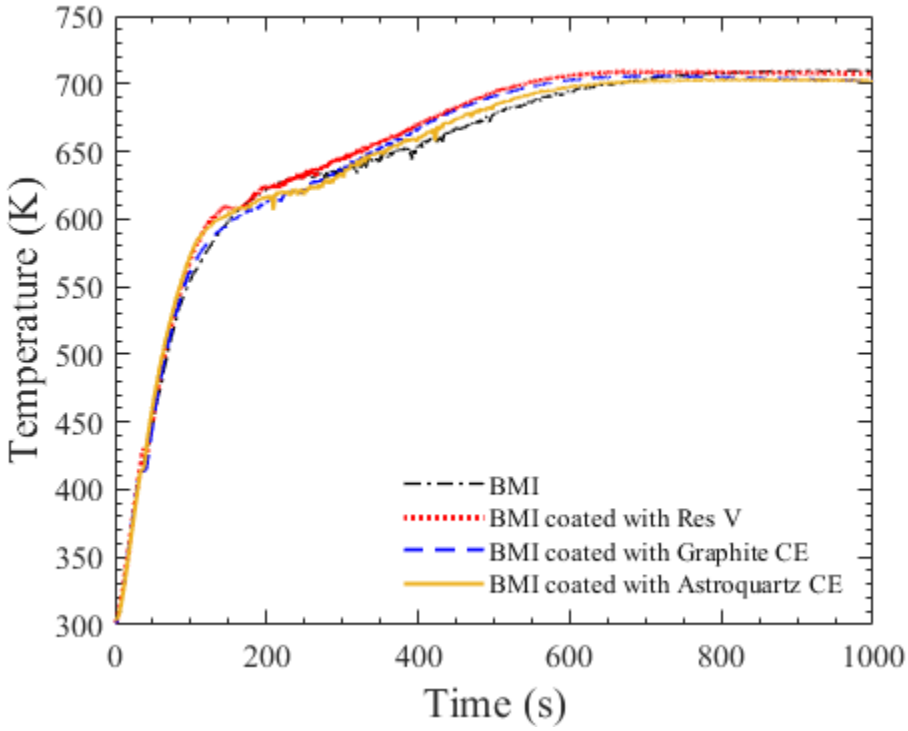

Figure 5.3: Comparison of the CAPA II back temperature of base BMI and BMI composites coated with barrier coatings applied at 65 kW m^{-2}.

It was observed that throughout testing that all samples, BMI and BMI coated with barrier coating, did not swell in any manner throughout testing. Due to the thin

coatings of the barrier coatings applied to the BMI swelling may not have been observed if the barrier coatings had been applied thicker.

5.2 CAPA II Modelling Conditions and Results

5.2.1 Test Conditions

The boundary conditions for the CAPA II were defined based on the collected temperature data above the sample surface during testing and below the bottom surface during testing. The boundary conditions were recorded for each test and were found to be similar enough to be averaged as a common set of boundary conditions for each test. It was assumed there was no conduction from the CAPA II to the sample due to the kaowool insulation on the sides of the sample. The boundary conditions for 65 kW m^{-2} are displayed in figures 5.4 and 5.5.

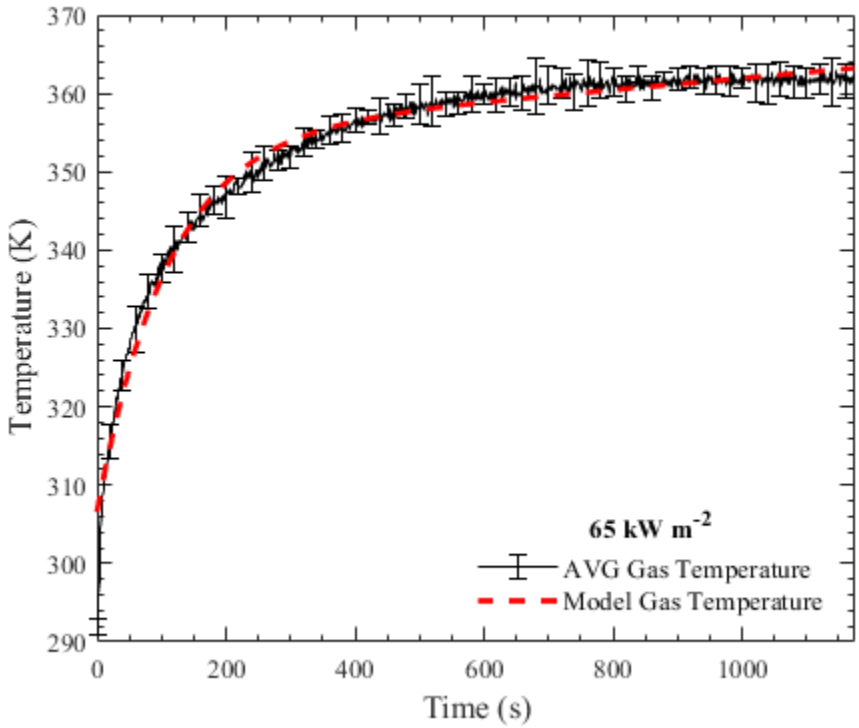

Figure 5.4: Average top boundary gas temperature data compared against modelled gas temperature for 65 kW m^{-2} CAPA II tests.

The top boundary conditions considered both the radiative and convective heating/losses that may occur. The top convective boundary condition model fits the experimental data well with the major discrepancies coming at around 200 to 400 seconds and the very end of the test. The top convective boundary condition model however still falls within the tight error bars of the average experimental data making it a good fit. The equation used to fit the temperature model (T^e) to the experimental temperature data was equation 5.2, where time is represented by t and the initial temperature (T_i) is defined as 291K.

$$T^e = T_1^e\,[\exp(T_2^e \times t)] + T_3^e\,[\exp(T_4^e \times t)] + T_i \tag{5.2}$$

The coefficients for the model for the gas temperature at 65 kW m^{-2} were as follows; T_1^e = 63.9 K, T_2^e = 1×10^{-4} s^{-1}, T_3^e = -48.3 K, T_4^e = -9.2×10^{-3} s^{-1}. To fully define the convective portion of the heating however a convection coefficient (h_c) must be defined, it was found for the boundary conditions of the CAPA II from a previous study that this could be defined using equation 5.3 [41]. Where h_c was found to be radially (r) dependent.

$$h_c = 2.97\ W\ m^{-2}K^{-1} + r(241.43\ W\ m^{-3}K^{-1}) \tag{5.3}$$

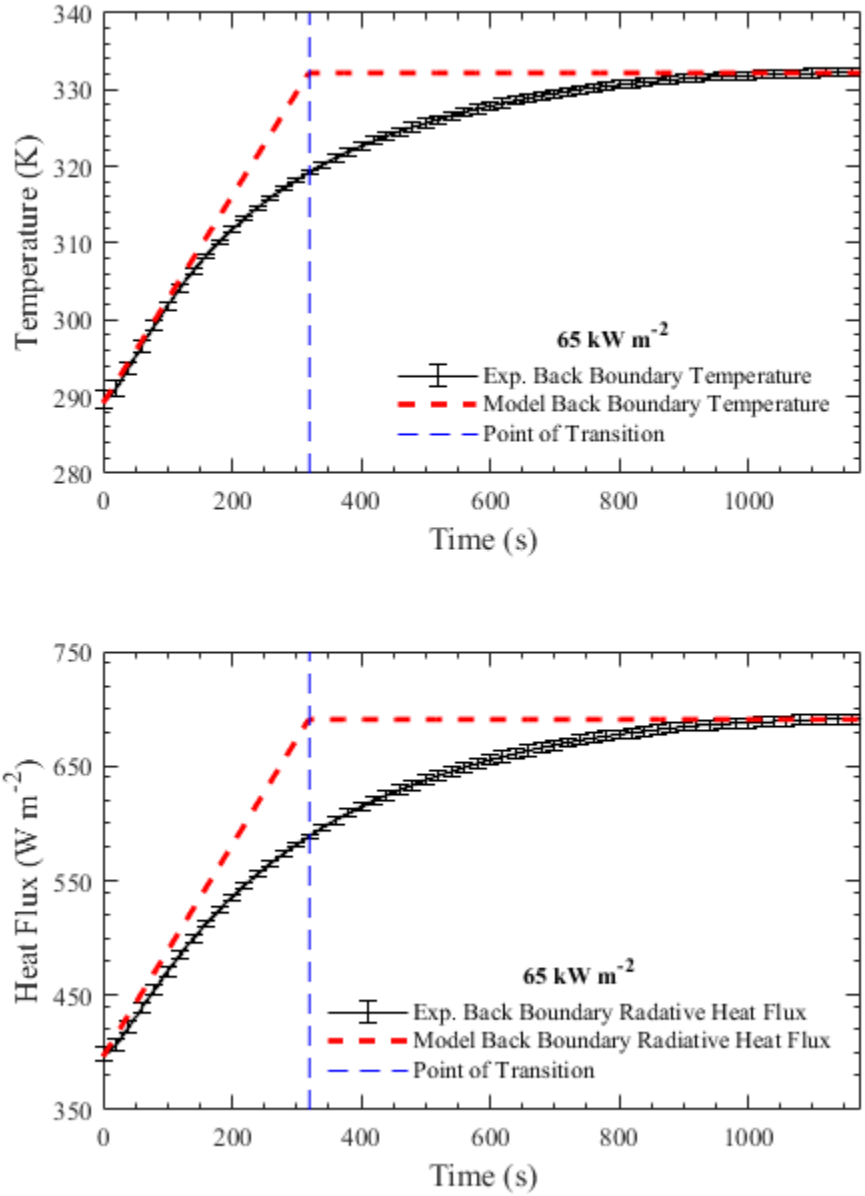

Figure 5.5: Representations of gas temperature and background radiative heat flux used to model the thermal boundary condition at then back surface in the 65 kW m^{-2} CAPA II tests.

The back boundary conditions considered both the radiative and convective heating/losses that may occur. To emulate this in ThermaKin a linear model must be used, the recorded experimental temperatures maximum value is considered the steady state temperature the model will reach, the initial slope of the temperature rise is then estimated by drawing a line tangent to the initial temperature data. The point of intersection between the two linear lines is then determined as the point of transition which for the 65 kW m^{-2} was at 320 seconds. The bottom boundary temperature was further defined by a convection coefficient determined to be weakly dependent on radial position but was averaged to be 4 W m^{-2} K^{-1} [41].

This process was repeated for the tests performed on BMI at 85 kW m^{-2} the results are displayed within figures 5.6 and 5.7 for the top and back boundaries respectfully.

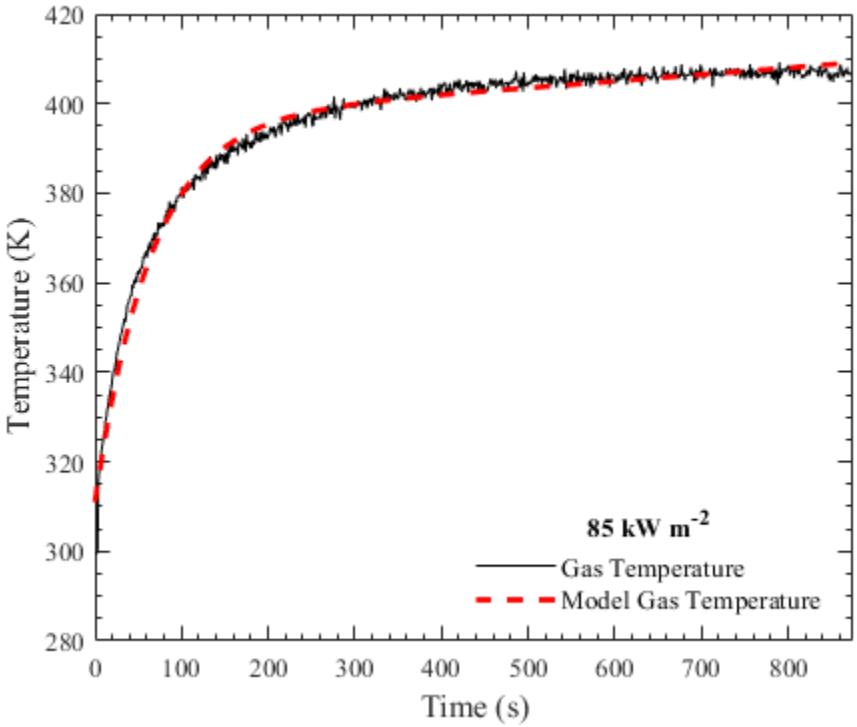

Figure 5.6: Average top boundary gas temperature data compared against modelled gas temperature for 85 kW m^{-2} CAPA tests.

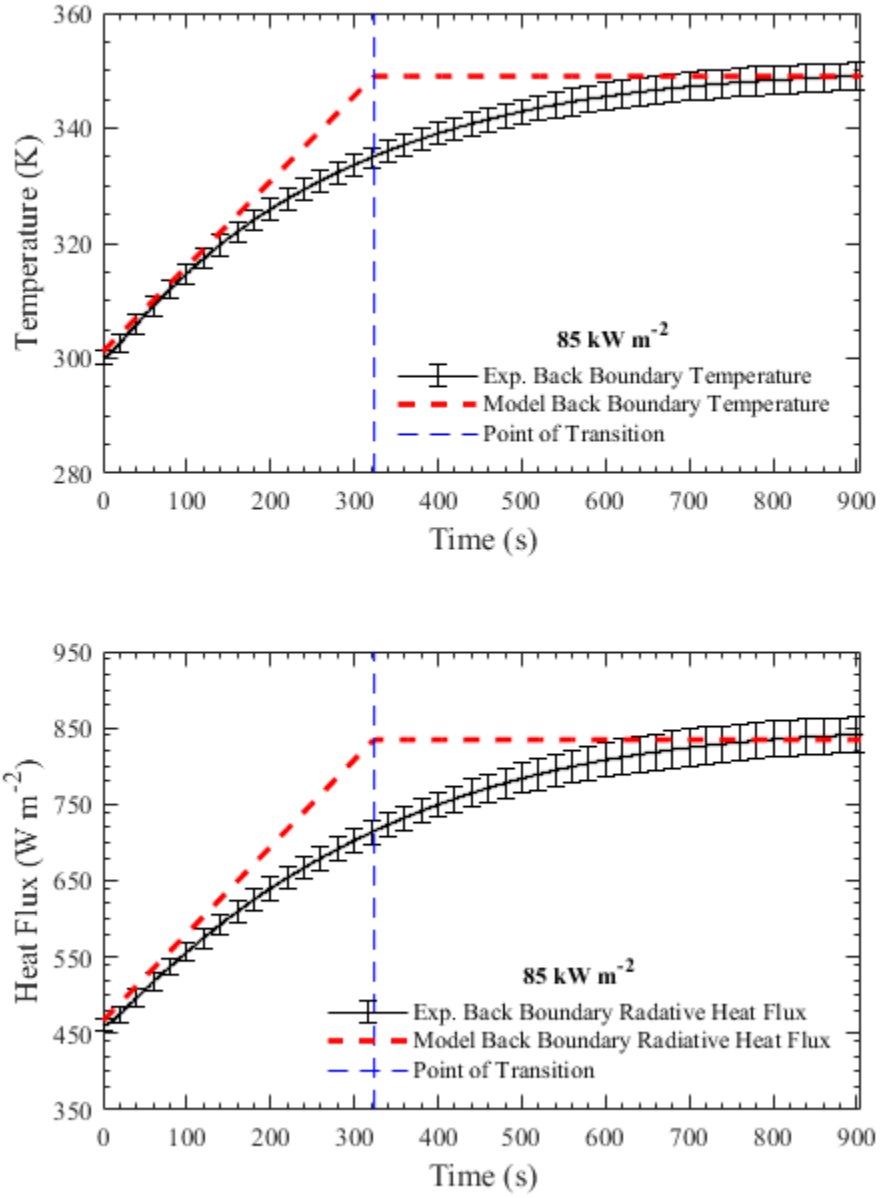

Figure 5.7: Representations of gas temperature and background radiative heat flux used to model the thermal boundary condition at then back surface in the 85 kW m^{-2} CAPA II tests.

The top boundary temperature model displayed in figure 5.6 utilized equation 5.2 to define the top boundary temperatures with the coefficients as follows;

T_1^e = 105.5 K , T_2^e = 1.3×10^{-4} s^{-1}, T_3^e = -85.5 K, T_4^e = -1.5×10^{-2} s^{-1}. The point of

transition defined for the figures displayed in figure 5.7 occurred at 324 seconds. Which was further defined using a convection coefficient (h_c) that is radially (r) dependent [41] this dependence is defined in equation 5.2.

All of the models were conducted using a spatial resolution of 1×10^{-5} and a time step of 0.001 s.

5.2.2 CAPA II Modelling Results

The modelling performed for all the CAPA II testing for the base composite BMI and composite barrier coatings was performed under the assumption that all of the composites held at a constant emissivity value of 0.92. This was justified for BMI as a single CAPA II test was performed with 0.92 emissivity high temperature paint was painted onto the top surface of BMI and the resultant MLR and back temperature curves bore no major discrepancies when compared to previous BMI tests. This value fell close to that of previous values determined in literature [42,43], helping further justify the decision for BMI. The emissivity values of the barrier coatings were held at 0.92. The absorption coefficient (α) for BMI and the barrier coatings was assumed to be a constant value of 10,000 $m^2\ kg^{-1}$. This value of α was chosen to not allow any significant amount of radiation to transfer through the sample, to emulate the tight weaved nature of the BMI and composite barrier coatings. As previously stated no notable change in volume occurred to the BMI sample during CAPA testing. To emulate this within the model the densities of the reactant within the reaction mechanism were multiplied by the stoichiometric coefficient of the product to determine the products density. For example for the 1st reaction for BMI the BMI_{int_1} density was calculated by multiplying BMI's density by Θ_1.

The inverse analysis performed on the CAPA II data for BMI and BMI coated with barrier coating, was first fit to the back temperature experimental data as shown in figure 5.8.

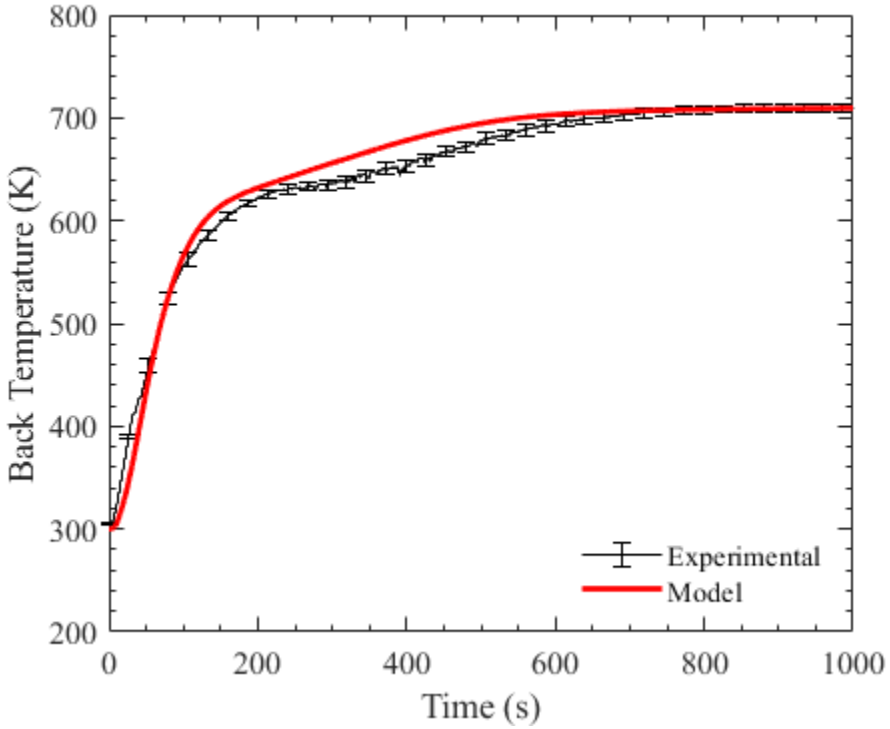

Figure 5.8: Average experimental back temperature at 65 kW m^{-2} applied heat flux for 4.6 mm thick BMI and corresponding ThermaKin model

The process of fitting the model back temperature to the experimental back temperature was performed by automated optimization. The back temperature model is a good fit to the experimental data. The largest discrepancies between the model and experimental data come between 300 to 500 seconds. This period of time during the test is unreliable in terms of the collected back temperature data due to gaseous pyrolyzates blocking the IR camera. It is expected if the camera had not been blocked by these gases, the temperature would have been higher than shown in the

experimental data shown in figure 5.8 during the period of 300 to 500 seconds. The results of the fitted model to the back temperature data are displayed in Table 5.1.

Table 5.1: Thermal conductivity and density for each of the solid components within the reaction model of BMI

Component	Thermal Conductivity ($W\ m^{-1}\ K^{-1}$)	Density ($kg\ m^{-3}$)
BMI	0.261	1513
BMI_{int_1}	0.05	1485
BMI_{int_2}	0.233	1301
BMI_{char}	$4.929 \times 10^{-10}\ T^{3}$	1177

Using the BMI model determined from fitting the experimental back surface temperature, the experimental MLR was compared to the models predicted MLR curve. The comparison plot is displayed within figure 5.9.

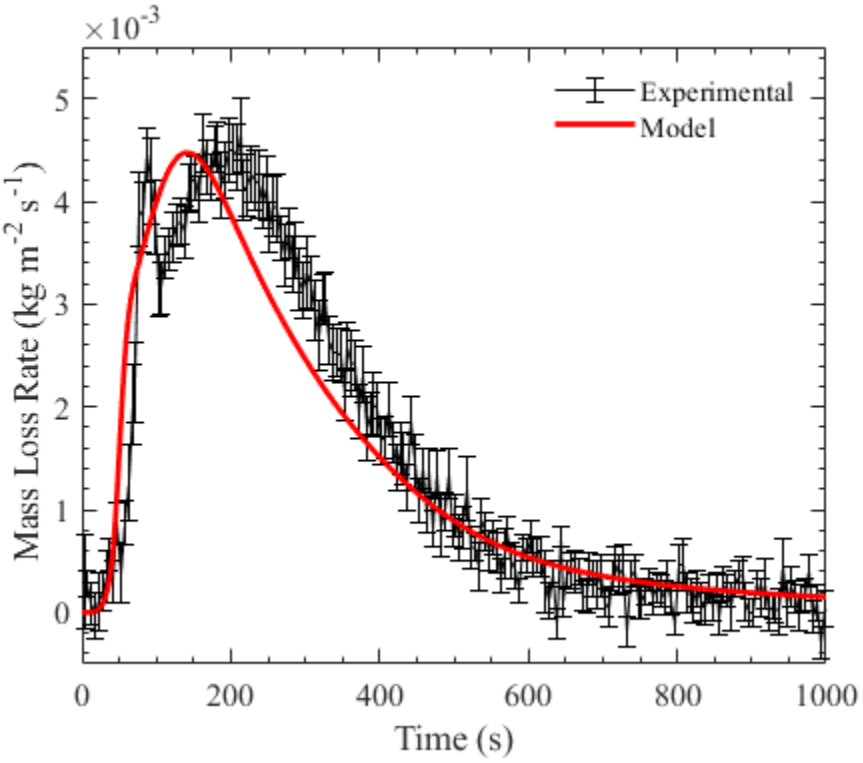

Figure 5.9: Average experimental MLR at 65 kW m^{-2} applied heat flux for 4.6 mm thick BMI and corresponding ThermaKin model

The models prediction of the MLR at 65 kW m^{-2} for BMI does a good job of capturing the experimental MLR. A minor discrepancy comes from the peak of the model MLR curve occurring roughly 25 seconds before the peak within the experimental data. With only minor discrepancies, and to further validate the model developed for BMI the model was run at 85 kW m^{-2} and compared to the corresponding experimental back temperature and MLR to further validate the model's versatility. The comparisons are displayed in figures 5.10 and 5.11.

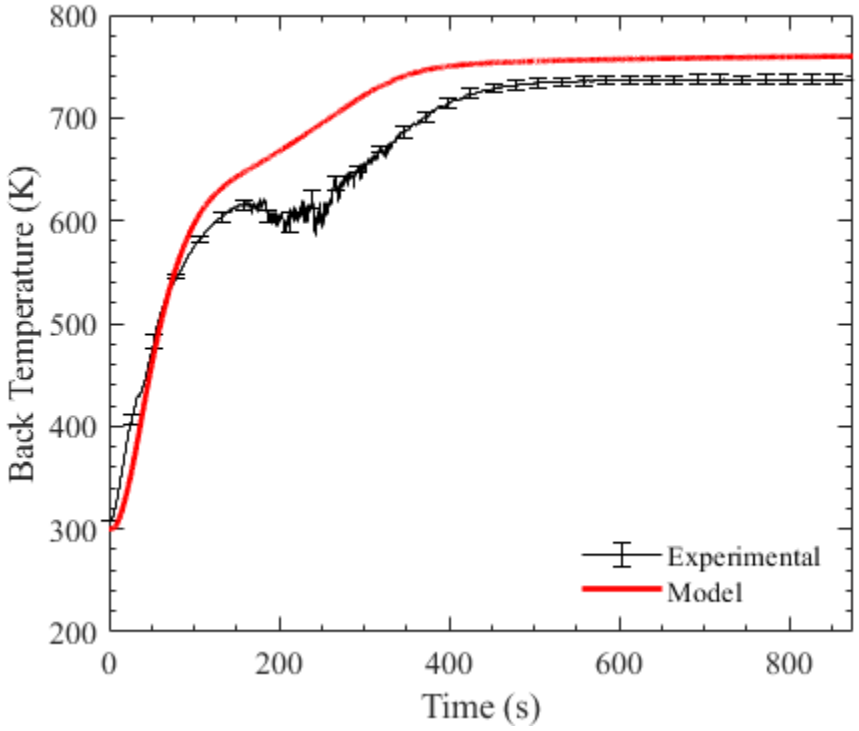

Figure 5.10: Average experimental back temperature at 85 kW m^{-2} applied heat flux for 4.6 mm thick BMI and corresponding ThermaKin model

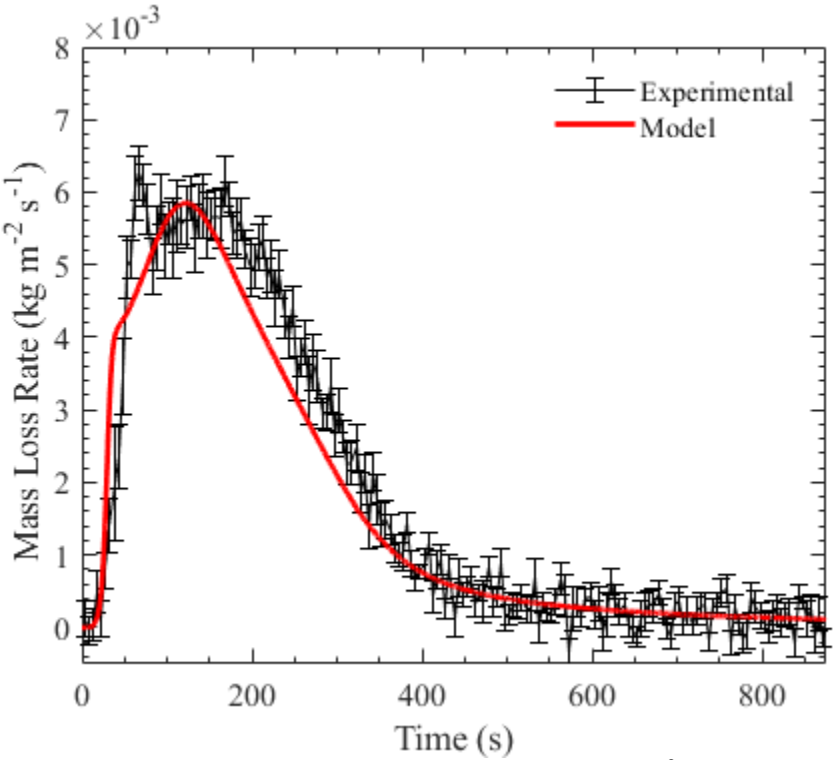

Figure 5.11: Average experimental MLR at 85 kW m^{-2} applied heat flux for 4.6 mm thick BMI and corresponding ThermaKin model

The model developed for BMI at 65 kW m^{-2} shows it still has the capability to predict results well when run at a different heat flux. The temperature model prediction for 85 kW m^{-2} shows a larger discrepancy from the experimental data then observed in the 65 kW m^{-2} tests. The maximum temperature is now approximately 20K higher than the experimental temperature, this difference is assumed smaller then displayed. As seen within the CAPA II performed on the BMI at 65 kW m^{-2} the IR camera is blocked by pyrolyzates gases and in the case of tests performed at 85 kW m^{-2} it is more severe. Due to this it is assumed that the model's prediction of the back temperature profile is potentially more accurate than the comparison in figure 5.10 alludes to. This is further supported by the MLR prediction by the model in figure 5.11 fitting the experimental MLR data just as well as it had for the 65 kW m^{-2} experimental data. With confidence in the BMI model it was then implemented into the models for resolving the BMI with barrier coatings CAPA II tests back surface temperature.

As previously stated, the models developed for the barrier coatings used the same assumptions as the BMI, meaning of all the components of each barrier coating were assumed to have an emissivity of 0.92 and an absorption coefficient of 10,000 m^2 kg^{-1}. The densities of the solid components for each of the barrier coatings was determined by the reactant's density multiplied by the product's stoichiometric coefficient. The models developed for the composite barrier coatings as displayed in figures 5.12 through 5.14. The developed models were built on the basis of the finished models for BMI with the addition of the composite barrier coatings now

being a part of the models in the measured thickness; 0.41 mm, 0.64 mm, and .41 mm for Res V, Graphite CE and Astroquartz CE respectfully.

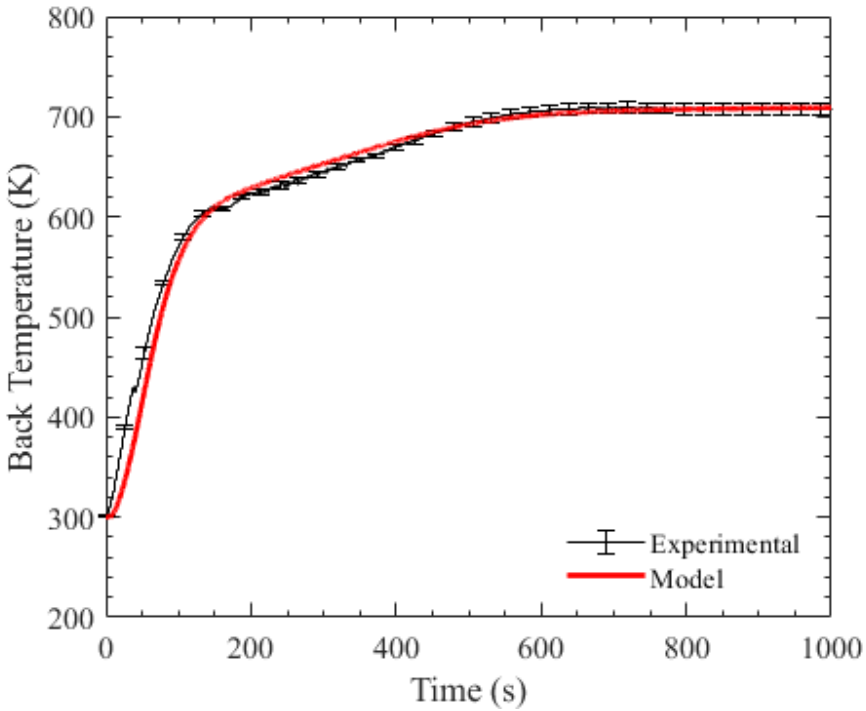

Figure 5.12: Average experimental back temperature at 65 kW m^{-2} applied heat flux for 0.4 mm thick Res V coating on 4.6 mm thick BMI and corresponding ThermaKin model

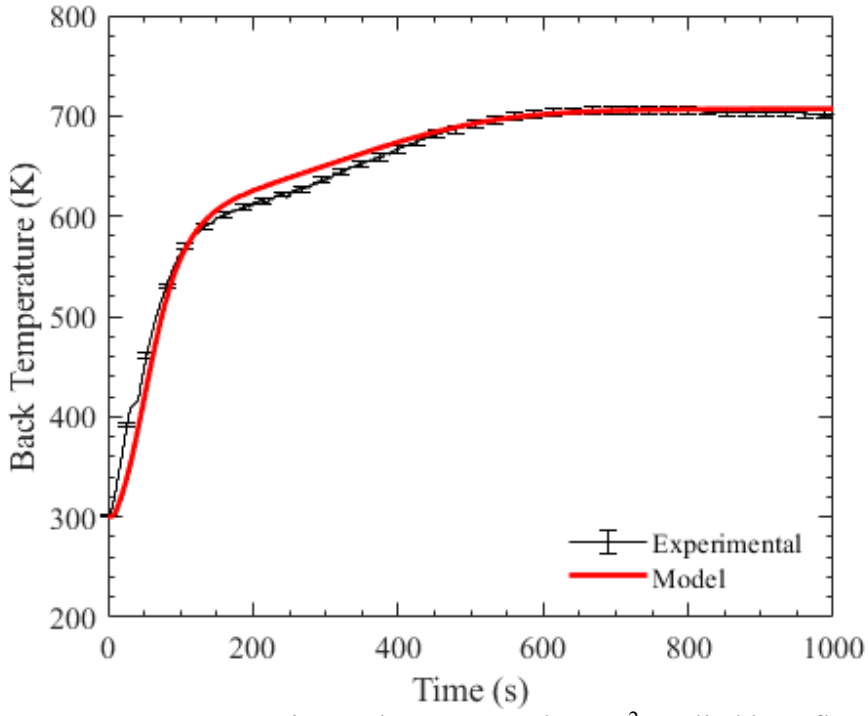

Figure 5.13: Average experimental MLR at 65 kW m^{-2} applied heat flux for 0.63 mm thick Graphite CE coating on 4.37 mm thick BMI and corresponding ThermaKin model

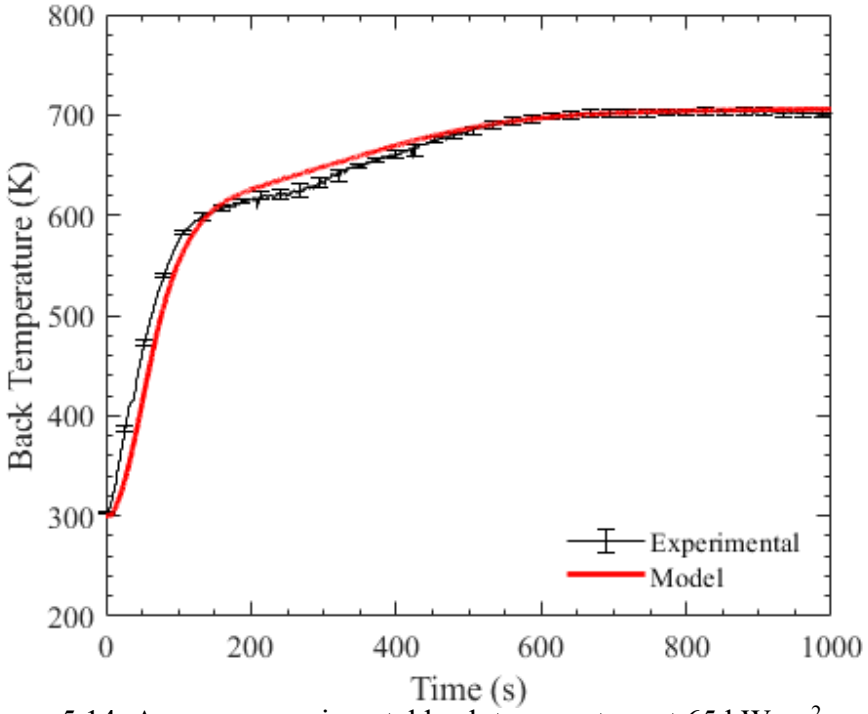

Figure 5.14: Average experimental back temperature at 65 kW m^{-2} applied heat flux for 0.46 mm thick Astroquartz CE coating on 4.54 mm thick BMI and corresponding ThermaKin model

The fits of the models for the back temperature for the barrier coatings show good agreement with their corresponding experimental data. The main discrepancies coming again from the portions of experimental data where the IR camera was blocked by pyrolyzate gases. The resulting conductivities determined from these fit models are displayed in table 5.2.

Table 5.2: Thermal conductivity and densities for each of the solid components within the reaction model for each composite barrier coating

CBC	Component	Thermal Conductivity ($W\ m^{-1}\ K^{-1}$)	Density ($kg\ m^{-3}$)
Res V	CBC	2.400	1893
	CBC_{int_1}	1.561	1746
	CBC_{int_2}	1.346	1598
	CBC_{char}	$4.683 \times 10^{-7}\ T^3$	1474
Graphite CE	CBC	2.402	1580
	CBC_{int_1}	0.124	1471.4
	CBC_{int_2}	1.356	1374
	CBC_{char}	$4.135 \times 10^{-10}\ T^3$	1310
Astroquartz CE	CBC	2.402	1987
	CBC_{int_1}	0.405	1832
	CBC_{int_2}	0.590	1714
	CBC_{char}	$1.059 \times 10^{-9}\ T^3$	1579

The values of thermal conductivity determined for the barrier coatings from the fitting of their back surface temperature would indicate that the barrier coatings are highly conductive to heat. Such a high conductivity for the barrier coatings is disadvantageous for their ability to protect the base composite of BMI. The potential reasons for the barrier coatings have such high thermal conductivities would be the thickness of the barrier coatings applied to BMI that were tested were too thin. Due to

the thin nature of the applied barrier coatings, it is assumed that the thermal conductivities were not fully resolved. The resulting MLR comparisons of the back temperature fit models vs the experimental MLR data for each composite barrier coating are displayed in figures 5.15 through 5.17.

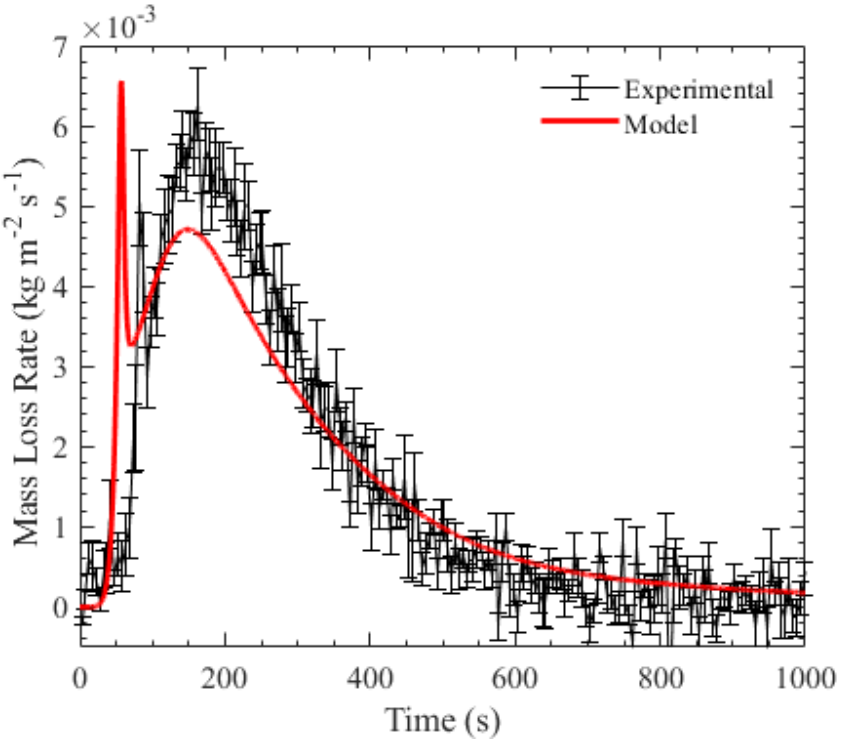

Figure 5.15: Average experimental MLR at 65 kW m^{-2} applied heat flux for 0.4 mm thick Res V coating on 4.6 mm thick BMI and corresponding ThermaKin model

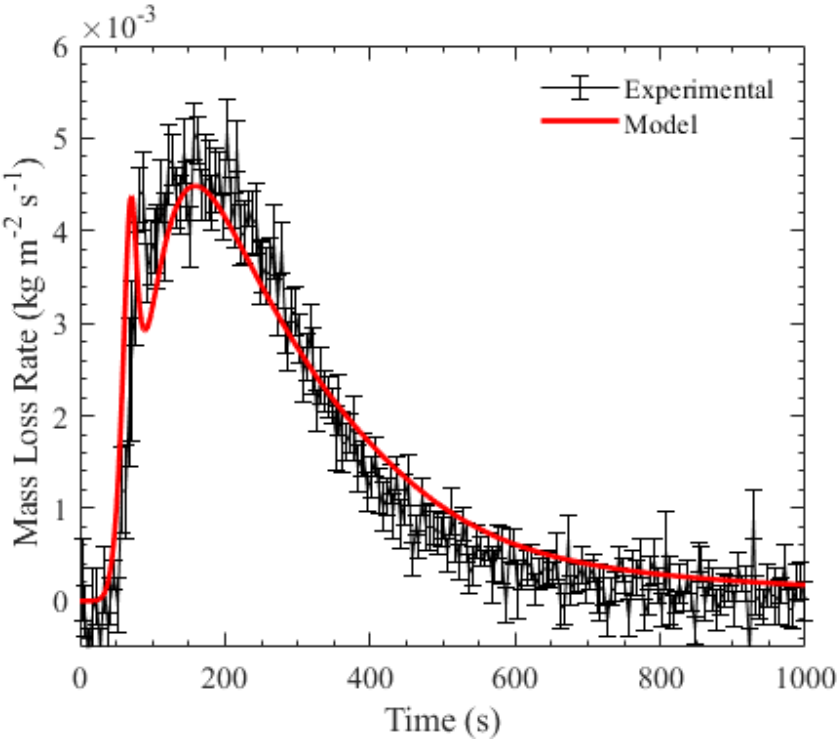

Figure 5.16: Average experimental MLR at 65 kW m^{-2} applied heat flux for 0.63 mm thick Graphite CE coating on 4.37 mm thick BMI and corresponding ThermaKin model

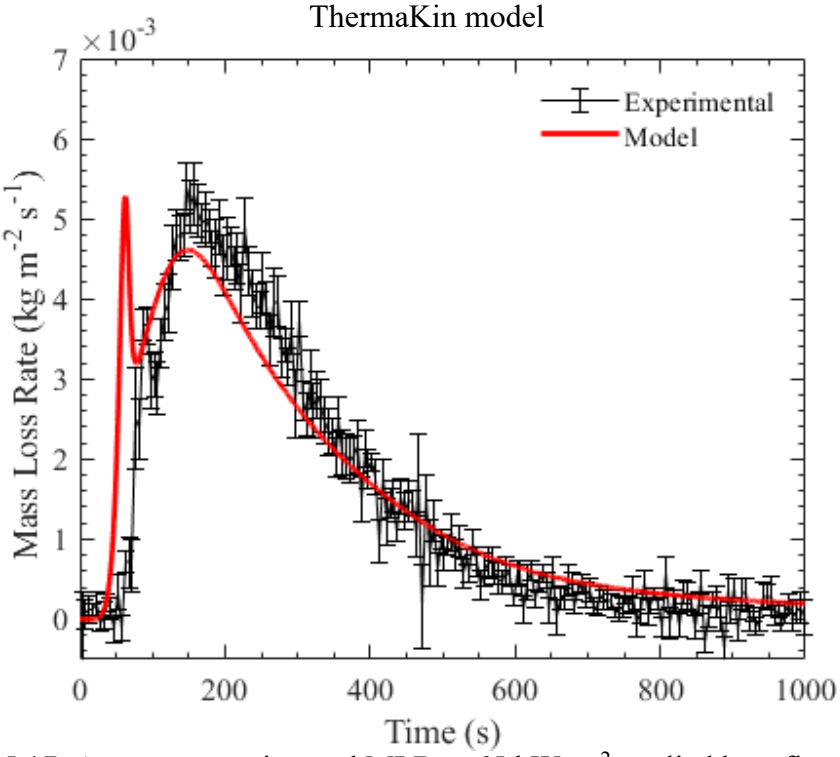

Figure 5.17: Average experimental MLR at 65 kW m^{-2} applied heat flux for 0.46 mm thick Astroquartz CE coating on 4.54 mm thick BMI and corresponding ThermaKin model

The predicted MLR curves shown for the BMI samples with the applied barrier coatings shows decent agreement when compared to their corresponding experimental data. Each predicted MLR curve shows a sharp peak occurring roughly 50 seconds after the beginning of the test is in large part due to the quick pyrolyzing of the barrier coatings. The sharp and quick MLR is in part due to the high conductivities of the barrier coatings as well as the thin nature of the barrier coatings. After this sharp peak in the MLR prediction, the main contribution the MLR was then the BMI. Both the BMI coated with Res V and BMI coated with Astroquartz CE model predictions for MLR share a much sharper initial MLR peak followed by a second smaller MLR peak that underpredicts the experimental MLR peaks. This is especially true when looking at the prediction for the BMI coated with Res V, an indication that the thermal conductivities may not be fully resolved and representative of Res V. The BMI coated in Graphite CE model prediction of the MLR shows the same two peak behavior as discussed for the other BMI coated predictions, however the second peak does a good job of predicting the corresponding experimental MLR. This may suggest that the thermal conductivities determined for Graphite CE are more resolved than the other coatings.

With the completion of the CAPA II testing and subsequent modelling BMI, Res V, Graphite CE and Astroquartz CE each have a completed set of parameters that define a pyrolysis model. This now allows for each material to be assessed for their flammability under any defined exposure to a source of heat that poses interest. With this capability and the assumption that the determined parameters for each material

are sufficiently resolved to allow for the exploration of the barrier coatings thicknesses impact on the performance of the BMI in a given scenario.

Chapter 6: Fuel Spill Fire Simulations

To explore further as to how the composite barrier coatings would operate under different situations multiple ThermaKin files were constructed with 0.4 mm, 0.8 mm, and 1.2 mm thick coatings applied to a 4.6 mm thick piece of BMI. This was constructed as a 1D simulation in ThermaKin. A simulation was also run with just BMI at a thickness of 4.6 mm as a control to compare to the results of the simulations run with BMI and a composite barrier coating. The models were designed to emulate an aircraft fuel fire test, since this material will be used specifically in aircraft. It was assumed that the flame would be directly impinging on the material and receiving only radiative heat. The back side of the material would be cooled at ambient temperature, assumed 22ºC, both convectively and radiatively. The front boundary radiative heat flux was modelled after a fuel fire report from the FAA that measured 136 kW m^{-2} of radiative heat flux coming from a 55 gallon 8 by 10-foot pool fire [44]. This was assumed to be considered an ultra-fast fire and therefore had a 75 second ramp period in which the fuel fire built up to its maximum heat flux of 136 kW m^{-2}. The results of these simulations are shown in figures 6.1 through 6.3.

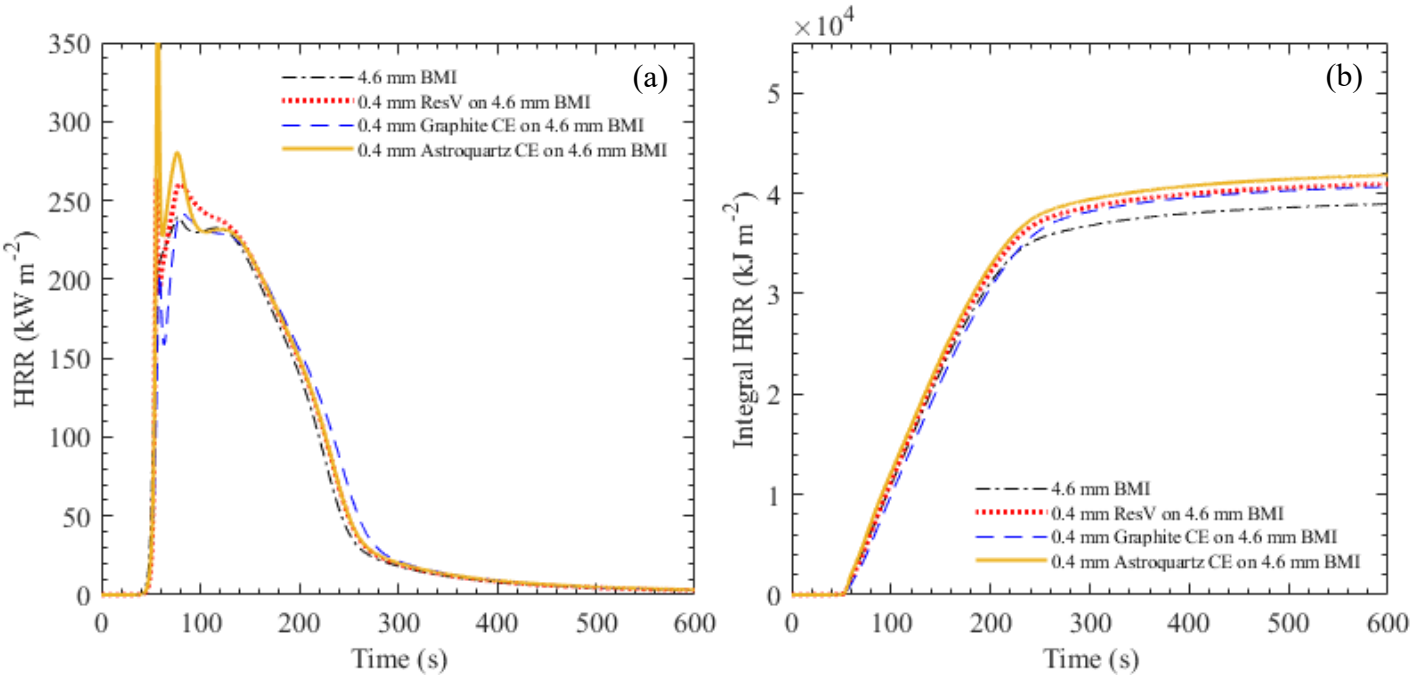

Figure 6.1: 4.6 mm thick BMI with 0.4 mm thick composite barrier coatings exposed to fuel fire conditions and their contributions to (a) HRR and (b) Integral HRR

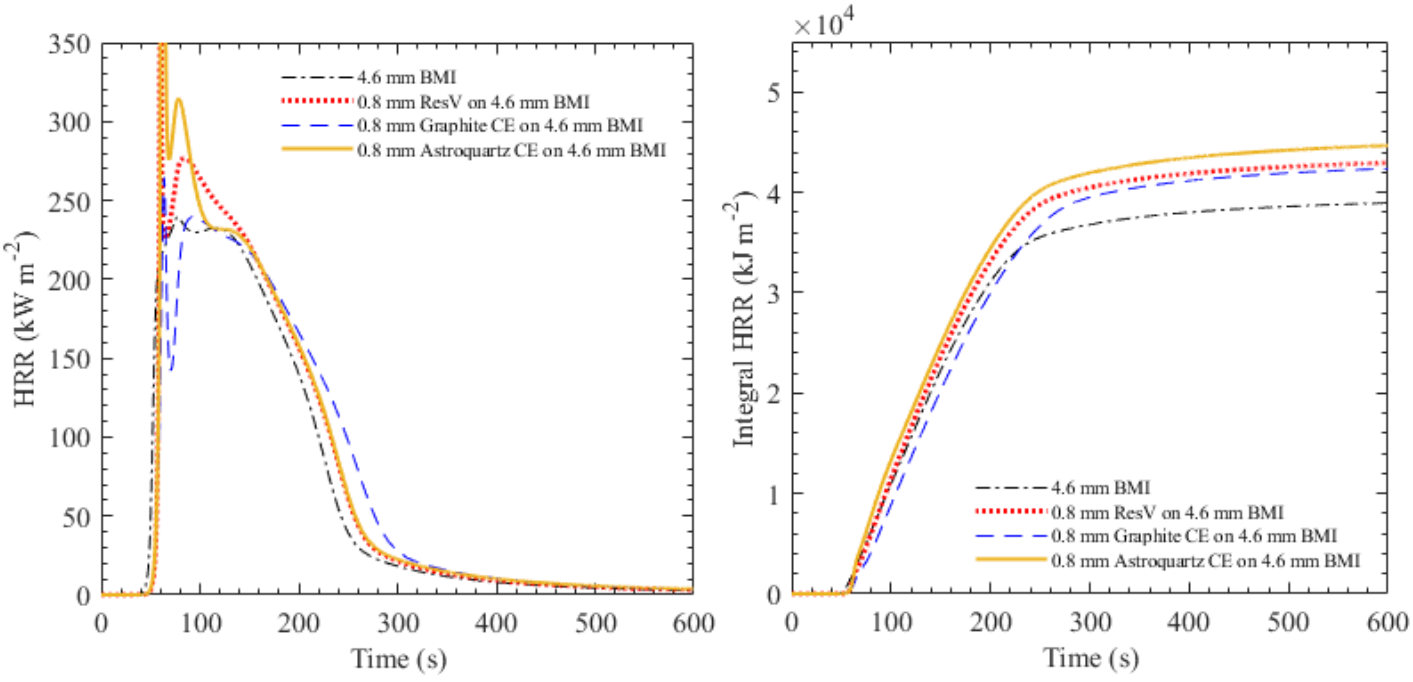

Figure 6.2: 4.6 mm thick BMI with 0.8 mm thick composite barrier coatings exposed to fuel fire conditions and their contributions to (a) HRR and (b) Integral HRR

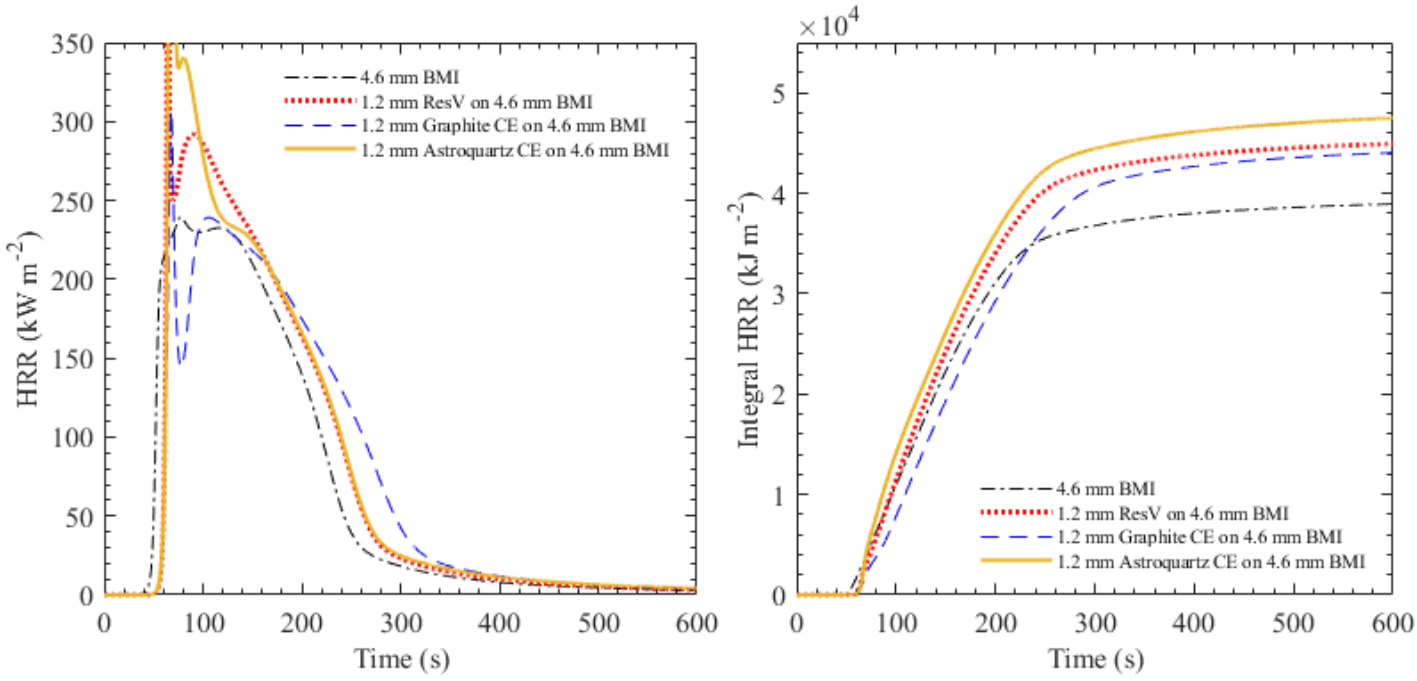

Figure 6.3: 4.6 mm thick BMI with 1.2 mm thick composite barrier coatings exposed to fuel fire conditions and their contributions to (a) HRR and (b) Integral HRR

Looking at the results of the figures the increase in thickness of the composite barrier coatings does provide a small delay in the start of mass loss and subsequent HRR, however from the HRR plots and made clear by the integral HRR plots the increase in thickness ends up increasing the fuel load and therefore just increases the total amount of heat released from the combination of BMI and composite barrier coatings. It is worth noting that the Graphite CE coating at 1.2 mm thickness performed the best out of all the composites, even reducing the HRR with respect to the pure BMI for a brief period of time during the burn time before then surpassing it again. Based on the properties derived from the milligram scale and CAPA II testing it would seem that the composite barrier coatings do not provide any significant thermal insulation/protection for BMI.

Chapter 7: Concluding Remarks

7.1 Conclusions

Within this study a base composite, BMI, was analyzed to create a fully developed pyrolysis model to determine its flammability properties to allow for further simulations to emulate what it may encounter as an aerospace composite. To try and aid the BMI's ability to withstand excessive heat three composite barrier coatings, Res V, Graphite CE, and Astroquartz CE were also analyzed and fully developed into pyrolysis models. The objective was then to understand what and if any of the provided composite barrier coatings would do as they were intended and improve upon the thermal response of the BMI. To determine this milligram-scale testing was performed for each composite individually to determine the kinetics and thermodynamics of thermal decomposition and combustion of gaseous pyrolyzates. CAPA II tests were then performed to define the thermal and mass transport of the materials. All of the collected milligram-scale and CAPA II tests were then inversely analyzed to create models to define the property set that makes up the full pyrolysis model. The models were created through the use of ThermaKin.

The milligram-scale testing and subsequent modelling provided an accurate representation of the milligram tests performed, TGA, DSC, and MCC. There is confidence in the milligram-scale results being fully resolved. When looking to the CAPA II results the priority was to fully resolve the BMI as it is the base composite, and without it being fully resolved the subsequent models with the applied composite barrier coatings would already lack confidence in their results. The models created for the BMI were fully resolved with confidence, however the results of the composite

barrier coatings did not seem to fully resolve in terms of the thermal conductivity. It is thought that this was due to the thin layer of composite barrier material that was layered upon the base BMI. The results were taken as is and used to run simulations of a airplane fuel fire with the composite barrier coatings varied in thickness on a uniform thickness of BMI. The result of the simulation showed that the coatings did not provide any benefit to the BMI but added to the fuel load and had increased outputs of HRR then that of just BMI with no coatings applied. Therefore, based on the experimental and modeling results from this study, it is recommended that none of the composite barrier coatings be used to try and bolster the fire resistance of the BMI.

7.2 Future Works

After analyzing the results of this study there is clear evidence that further work can be done to validate and further the development of the composite base coatings. Due to the thin nature of the composite barrier coatings that were applied to the BMI it was unclear if the thermal conductivity had been fully resolved. It would be recommended that CAPA II testing be redone for Res V, Graphite CE, and Astroquartz CE composite barrier coatings. The coatings should be applied to a uniform thickness of BMI with a corresponding uniform thickness of the composite barrier coatings applied in a thicker layer than they were within this study. It may be beneficial to perform testing on the composite barrier coatings by themselves within the CAPA II, but these tests should not be performed in replacement of the BMI samples with the applied composite barrier coatings, as to not miss any important interactions taking place where the BMI and composite barrier coating meet. The

CAPA II testing should be conducted with care, especially when preparing the sample with the kaowool rings to try and prevent any off gassing and mass loss from them.

Future work performed with these composite barrier coatings should be focused on further resolving their thermal conductivities, focusing on improving their thermal conductivities and potential other testing methods to determine the effectiveness of the coatings.

Appendices

A.1: Composite barrier coatings manufacture and production details

A.1.1 BMI

The fiber material IM7 graphite is produced by Hexcel and produced to the Hexcel grade specification of HS-CP-5000 and the carbon fiber being qualified to NMS 818 Carbon Fiber specification. The BMI composite test materials were fabricated in accordance with the Lockheed martin material specification LMA MB001, which is described in the Joint Striker Fighter (JSF) program document 2ZZZ00005 – Composite Ply Prepreg, BMI. Once processing the material had finished the BMI test panels were evaluated by ultrasonics NDI to confirm the quality of the panels to ensure there was not porosity or delamination's occurring with the layup.

A.1.2 Res V

Trifunctional phenol trans-resveratrol was synthesized from glucose using metabolically engineered yeast. The trans-Resveratrol was next photo-chemically converted to cis-resveratrol and then chemically converted to a tricyanate ester (cis-ResVCy) [34,35]. To allow for a more efficient processing of the Cis-ResVCy its polymer nest was blended with the lower viscosity PT30 Cyanate Ester manufactured by Lonza. These were then manufactured into three different blends of which the 70/30 CisResVCy/PT30 was tested within this study.

A.1.3 Graphite CE

The fiber, IM7 graphite, has been qualified to NMS 818 Carbon Fiber Specifications and is manufactured to Hexcel aerospace grade specification HS-CP-5000.

A.2: Fabrication and Curing Processes

A.2.1 Fabrication of Composite Barrier Coatings

The fabrication for all the barrier coatings (Res V, Graphite CE, and Astroquartz CE) were all the same and are explained within this section. The process involved was a wet layup process. The first step of the process was 12 by 12-inch sheets of reinforcement fabrics being cut and dried in an oven held at 90ºC with air circulation. The reinforcement fabrics were allowed to dry for a minimum of 3 days. The next step involved measuring out roughly 30 grams of PT30 in a glass beaker and then proceed to melt the PT30 within a held vacuum at 80ºC. This was done to lower the resins viscosity and outgas the polymer. The 80ºC value was determined from previous studies showing that the PT30 could have its viscosity lowered without risk of prematurely curing. Proceeding this a Teflon release film was place on a hot plate held at 100 ºC and then a 12 by 12-inch piece of the dried reinforcement fabric is placed on the hot plate. The 30 grams of PT30 is then removed from the oven and poured onto the fabric, this process was repeated until the laminate had reached a layering of 8 ply.

A.2.2 Curing Process for Composite Barrier Coatings

The curing process for the barrier coatings was performed the same way for the Graphite CE and Astroquartz CE, but not for the Res V. The Res V being a new material is cured using a curing schedule developed at NAWCWD, which has not public information at this time. The curing process discussed within this section now solely pertains to Graphite CE and Astroquartz CE.

The impregnated plys were laid up on an Al plate covered with a sheet of Release Ease® 234 TFNP non-porous Teflon release film. Damming tape was placed all around the perimeter of the ply stack to prevent any excess resin from leaking outside of the damming area. A sheet of nonporous Teflon release film was placed over the dam and ply stack with at least an excess of 1 inch of film around the perimeter of the dam. One sheet of 1/8 inch thick NBR_3000-10 breather fabric was placed over the entire release film area. This was then vacuum bagged with 450-1 high temperature vacuum tape and Capran® HS6262 vacuum bagging film. The impregnated ply's were vacuum cured in an air circulating oven. The cure cycle used was the recommendation from the vendor, this consisted of the following; From room temperature the oven was raised to 150ºC at a rate of 2.8ºC/min and then held for one hour. After the one hour hold at 150ºC the temperature is then increased to 200ºC at a rate of 2.8ºC/min. The oven is then held at 200ºC for 3 hours. After this process the excess resin between the ply stacks and the silicon dam is removed and the material is then post cured in an air circulating oven at 260ºC for 3 hours.

Bibliography

[1] R. Groh, A Brief History of Aircraft Structures, Aerospace Engineering Blog (2012). https://aerospaceengineeringblog.com/aircraft-structures/

[2] M. Wilhelm, Aircraft applications, ASM Handbook, Vol 21: Composites, ASM International, 2001.

[3] M. Jawaid, M. Rasheed, N. Saba, R. Siakeng, N. Saba, and S. Waheedullah Ghori, The Role of advanced Polymer Materials in Aerospace, Sustainable Composites for Aerospace Applications (2018) 19-34. doi: http://dx.doi.org/10.1016/B978-0-08-102131-6.00002-5

[4] S. Ahmed Atique, A. Shahriar Nafi, and N. Nawal Probha, Polymer composites: a blessing to modern aerospace engineering, International Conference on Mechanical, Industrial, and Energy Engineering (2014).

[5] E. Bubert, C. Kothera, K. Lee, N.M. Wereley, and B. Woods, Design and Fabrication of a Passive 1D Morphing Aircraft Skin, Journal of Intelligent Material Systems and Structures Vol 21, Issue 17, 2010. doi: https://doi.org/10.1177%2F1045389X10378777

[6] R. Bortolin, S. Joshi, M. Keihl, B. Sanders, and Z. Tidwell, Mechanical properties of shape memory polymers for morphing aircraft applications, Proc. SPIE 5762, Smart Structures and Materials 2005: Industrial and Commercial Applications of Smart Structures Technologies, (5 May 2005); doi: https://doi.org/10.1117/12.600569

[7] S. Rauscher, Testing and Analysis of Shape-memory Polymers for Morphing Aircraft Skin Application, University of Pittsburgh (2008).

[8] G. Burt, S. Galloway, S. Hallet, C. Jones, M. Jones, L. Kawashita, and P. Norman, Electrical model of carbon fibre reinforced polymers for the development of electrical protection systems for more-electric aircraft, 2016 18th European Conference on Power Electronics and Applications (EPE'16 ECCE Europe), Karlsruhe, 2016, pp. 1-10.
doi: 10.1109/EPE.2016.7695300.

[9] R. Ebewele, Polymer Science and Technology, (2000)

[10] D. Bower, An Introduction to Polymer Physics, Cambridge University Press (2012).
doi: https://doi.org/10.1017/CBO9780511801280

[11] F. Jin, X. Li, S. Park, Synthesis and application of epoxy resins: A review, J. Ind. Eng. Chem. (2015) , 29, 1–11.

[12] S. Kesarwani, Polymer Composites in Aviation Sector, Department Of Plastic Engineering, International Journal of Engineering and Technical Research, Volume 6 (2017).
doi: http://dx.doi.org/10.17577/IJERTV6IS060291

[13] R. Wang, S. Zheng, and Y. Zheng “Polymer Matrix Composites and Technology” Woodhead publishing 2011

[14] C. Lautenberger, C. Fernandez-Pello, Generalized pyrolysis model for combustible solids, Fire Saf. J. 44 (2009) 819–839.
doi:10.1016/j.firesaf.2009.03.011.

[15] K. McGrattan, S. Hostikka, R. McDermott, J. Floyd, M. Vanella, Sixth Edition Fire Dynamics Simulator Technical Reference Guide Volume 1 Mathematical Model 6.3, 1 (2015)

[16] S.I. Stoliarov, R.E. Lyon, Thermo-kinetic model of burning for pyrolyzing materials, in: Fire Saf. Sci., 2008. doi:10.3801/IAFSS.FSS.9-1141.

[17] S. Stanislav, I. Leventon, and R. Lyon, Two-dimensional model of burning for pyrolyzable solids, Fire and Materials International Journal (2013). https://doi.org/10.1002/fam.2187

[18] J. Swann, and S. Stoliarov, A Comprehensive Characterization of pyrolysis and combustion of rigid poly(vinyl chloride) using two-dimensional modeling: A Relationship between Thermal Transport and The Physical structure of the Intumescent Char (2019). doi: https://doi.org/10.13016/6kol-uubx

[19] L. Ilcewicz, Past Experiences and Future Trends for Composite Aircraft Structure, Montana State University Seminar (2009). https://www.montana.edu/dcairns/documents/composites/11-10-09li.pdf

[20] F. Findik, and Y. Yillikci, A Survey of Aircraft Materials: Deign for Airworthiness and Sustainability, Periodicals of Engineering and Natural Sciences (2013). doi: http://dx.doi.org/10.21533/pen.v1i1.13

[21] A. Labidi, Boeing 787 Dreamliner Represents Composites Revolution (2020)

[22] A. Horner, Aircraft Materials Fire Test Handbook, FAA report DOT/FAA/AR-00/12, April 2000.

[23] FAR part 25, https://www.ecfr.gov/cgi-bin/text-idx?node=14:1.0.1.3.11

[24] A. Gibson, and A. Mouritz, Modelling the Thermal Response of Composites in Fires, Fire Properties of Polymer Composite Materials (2006) 133-161. doi: http://dx.doi.org/10.1007/978-1-4020-5356-6

[25] J.B. Henderson, J.A. Wiebelt and M.R. Tant, A model for the thermal response of polymer composite materials with experimental verification, Journal of Composite Materials, 1985; 19:579-595

[26] S. Case, P. Des Jardin, S. Feih, E. Kandare, B. Lattimer, Z. Mathys, and A. Mouritz, Review of fire structural modelling of polymer composites, Composites: Part A 40 (2009) 1800–1814. doi: https://doi.org/10.1016/j.compositesa.2009.09.001

[27] B. Lattimer, and J. Trelles, Modelling thermal degradation of composite materials, Fire and Materials international journal (2006). doi: https://doi-org.proxy-um.researchport.umd.edu/10.1002/fam.932

[28] M. McKinnon and S. Stoliarov, Pyrolysis Model Development for a Multilayer Floor Covering, Influence of Thermo-Physical and Thermo-Optical Properties on the Fire Behavior of Polymers (2015). doi: https://doi.org/10.3390/ma8095295

[29] J. Quintiere, R. Walters and S. Crowley, Flammability properties of aircraft carbon-fiber structural composite.Technical report, Report no. DOT/FAA/AR-07/57, October 2007, pp. 8–72, https://www.fire.tc.faa.gov/pdf/07-57.pdf

[30] Kim, M. and Quintiere, J.G., Predicting Polymer Burning Using TGA/DSC, 5th Int. Seminar on Fire and Explosion Hazards, Edinburgh, 23-27 April 2007.

[31] P. Desjardin, A. Barra Dodd, and M. McGurn, Thermal Modeling of Carbon-Epoxy Laminates in Fire Environments, 10th International Symposium on Fire Safety Science, June 19, 2011 - June 24, 2011.
doi: http://dx.doi.org/10.3801/IAFSS.FSS.10-1193

[32] M. McKinnon, Y. Ding, S.I. Stoliarov, S. Crowley and .R. Lyon, Pyrolysis model for a carbon fiber/epoxy structural aerospace composite, Journal of Fire Sciences 2017, Vol. 35 (I) 36-61

[33] S. Stanislav, I. Leventon, and R. Lyon, Two-dimensional model of burning for pyrolyzable solids, Fire and Materials International Journal (2013).
https://doi.org/10.1002/fam.2187

[34] S. Stoliarov, and J. Li, Parameterization and validation of pyrolysis models for polymeric materials. Fire Technol 2016; 52: 79–91.
doi: http://dx.doi.org/10.1007/s10694-015-0490-1

[35] E. Kandare, and B. Kandola, Composites having improved fire resistance, Advances in Fire Retardant Materials, (2008), 398-442.
doi: https://doi.org/10.1533/9781845694701.3.398

[36] FAR part 25, https://www.ecfr.gov/cgi-bin/text-idx?node=14:1.0.1.3.11

[37] S.I. Stoliarov, R.E. Lyon, Thermo-kinetic model of burning for pyrolyzing materials, in: Fire Saf. Sci., 2008. doi:10.3801/IAFSS.FSS.9-1141.

[38] G. Fiola, and S.I. Stoliarov, Improving Inverse Analysis of Pyrolysis Model Paramaterization using Hill Climbing Algorithms, Masters Thesis (2019).
doi: https://doi.org/10.13016/73q9-6f3r

[39] G. Fiola, D. Chaudhari, and S. Stoliarov, Comparison of Pyrolysis Properties of Extruded and Cast Poly(methylmethacrylate), Fire Safet Journal: Vol 120 (2021) doi: https://doi.org/10.1016/j.firesaf.2020.103083

[40] J. Li, J. Gong, and S.I. Stoliarov, Gasification experiments for pyrolysis model parameterization and validation. Int J Heat Mass Tran 2014; 77: 738–744

[41] J. Swann, Y. Ding, M. McKinnon, and S. Stoliarov, Controlled atmosphere pyrolysis apparatus II (CAPA II): A new tool for analysis of pyrolysis of charring and intumescent polymers, Fire Safety Journal 91 (2017) 130-139. doi: https://doi.org/10.1016/j.firesaf.2017.03.038

[42] Hubbard JA, Brown AL, Dodd AB, et al, Carbon fiber composite characterization in adverse thermal environments, SANDIA report, Report no. SAND2011-2833 (2011) http://prod.sandia.gov/techlib/access-control.cgi/2011/112833.pdf

[43] Boulet P, Brissinger D, Collin A, et al, On the influence of the sample absorptivity when studying the thermal degradation of materials, Materials 2015; 8: 5398–5413

[44] T. Marker, Full-scale Test Evaluation of Aircraft Fuel Fire Burnthrough Resistance Improvements, FAA Report no. DOT/FAA/AR-98/52 (1999).